Annu. Rev. Earth Planet. Sci. 2001. 29:419–60

PHYSICS OF PARTIALLY SATURATED POROUS MEDIA: Residual Saturation and Seismic-Wave Propagation

Xun Li[1], Lirong Zhong[2], and Laura J Pyrak-Nolte[2,1]
[1]Department of Earth and Atmospheric Sciences and [2]Department of Physics, Purdue University, West Lafayette, Indiana 47907-1396; e-mail: ljpn@physics.purdue.edu

Key Words seismic wave attenuation, tomography

■ **Abstract** In this paper, we present a review of seismic-wave propagation in fluid-saturated and partially saturated porous media. Seismic-wave velocity and attenuation are affected by the degree of saturation and the spatial distribution of fluids within the medium. Attenuation mechanisms include local and global flow as well as energy loss caused by scattering. We also present results from acoustic tomography of unconsolidated porous media with residual paraffin saturation. The acoustic attenuation was found to be sensitive to the grain- and subgrain-scale (microscale) distribution of residual saturation; in other words, the residual saturation behaves like soft cement that locally stiffens grain contacts and creates heterogeneity that results in scattering. The effect of microscale phenomena on multigrain scale (macroscale) measurements of seismic-wave attenuation and velocity cannot be ignored.

INTRODUCTION

A goal of seismic exploration and monitoring is to delineate the structure of subsurface reservoirs and to delineate the distribution of phases within these reservoirs. Subsurface oil reservoirs often contain multiple fluid phases, such as gas, oil, and water. Because of these multiple phases and the complex nature of porous rock, residual amounts of each fluid phase remain in the pore space of the rock after oil production. In primary oil recovery, water is commonly injected into oil reservoirs to displace the oil from the pores within the rock. Because the capillary forces are large compared to the viscous forces, between 20% and 60% of the oil remains trapped within the rock as residual saturation. This can lead to significant economic loss. Maximum mobilization of the trapped oil is the goal of enhanced oil recovery.

Similarly, cleanup of a contaminant in subsurface aquifers is not successful if residual amounts of the contaminant are left in the pore space of the aquifer. Non-aqueous-phase liquids (NAPLs) are common contaminants in soil and aquifers.

0084-6597/01/0515-0419$14.00

NAPL spills or leaks generally migrate downward through the vadose (unsaturated) zone under gravitational forces, eventually reaching the water table. If the NAPL is less dense than water (LNAPL), it floats on the water table. If the NAPL is denser than water (DNAPL), it displaces water and penetrates the aquifer. During the migration process, NAPL gets trapped as blobs in soil or aquifer rock, resulting in residual saturation. Residual NAPL in soil and aquifers usually serves as a lasting source of groundwater contamination. Remediation of residual NAPL is therefore an important issue in environmental restoration.

Thus, a goal of geophysical monitoring in oil and gas production and contaminant cleanup is to determine the amount and spatial distribution of residual saturation of oil in an oil reservoir or contaminants in an aquifer. A considerable volume of work has been conducted on seismic-wave propagation through sediments and sedimentary rocks. Both laboratory measurements and theoretical calculations show that seismic-wave velocities and attenuation are strongly influenced by stress-induced changes to the grain microstructure and by the presence of pore fluids. These two factors also interact with each other during seismic-wave propagation, resulting in a local or global flow of fluids. To determine if seismic methods can be used to delineate the spatial distribution of residual fluid saturation, it is important to understand the mechanisms and material properties that can produce residual saturation in a porous medium and how these material properties also affect seismic-wave propagation.

Residual saturation in a porous medium occurs during the flow of two or more immiscible fluids. Immiscible fluids are fluids that do not mix and do maintain a well-defined interface between the two fluid phases. Multiphase flow of immiscible fluids in porous media is often encountered in relatively shallow subsurface layers, when soil or aquifers are contaminated by organic liquids and when the organic liquids are removed during environmental remediation. Multiphase flow is also commonly seen in oil reservoirs during petroleum recovery operations, in which water and gas are simultaneously produced along with oil. In discussing two immiscible fluids in a porous medium, one phase is often referred to as the wetting phase and the second fluid is referred to as the nonwetting phase. The scientific definition of a wetting phase is the fluid that makes a contact angle of $<90^\circ$ when in contact with a solid and another fluid (Scheidegger 1974); conversely, the definition of the nonwetting phase is the fluid that makes a contact angle of greater than 90° when in contact with a solid and another fluid.

Scheidegger (1974), from experimental measurements, described three general regimes of fluid saturation in a porous medium with two immiscible liquid phases in multiphase flow processes: a pendular regime, a funicular regime, and a complete saturation regime. The pendular regime refers to discrete rings of liquid at interparticle contact points (Figure 1*a*). Because the pendular bodies of liquid do not touch each other, there is no possibility of flow for that phase. The degree of saturation of that phase is usually very low. With reference to aquifers, liquids are retained in the pendular configuration in regions of unsaturated soil at heights well above the water table. In oil reservoirs, water or oil may form pendular rings

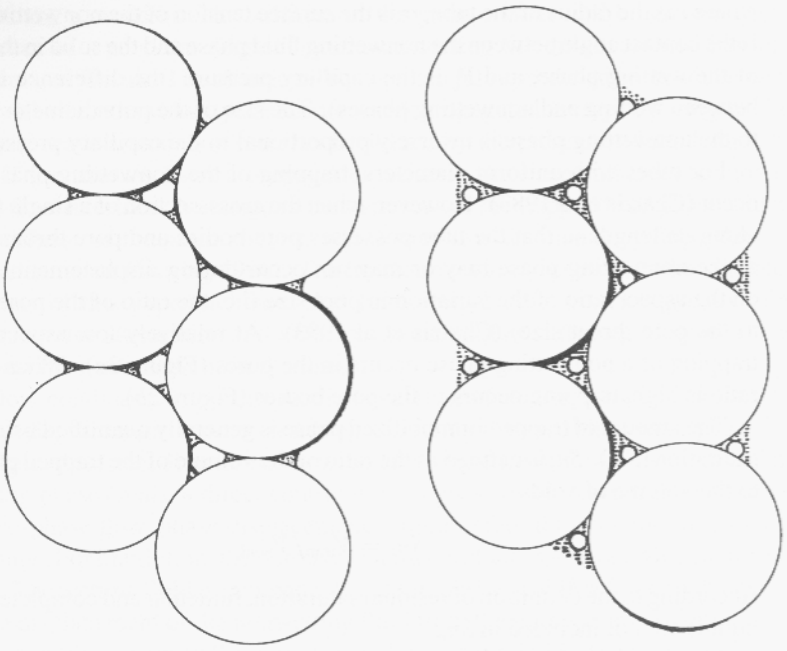

Figure 1 Drawing of pendular (*a*) and funicular (*b*) saturation regimes for an idealized porous medium consisting of packed spheres. (Based on Scheidegger 1974.)

depending on the surface properties of the reservoir rock, (i.e. oil-wet or water-wet rock). The funicular regime of saturation (Figure 1*b*) occurs when the porous medium has an intermediate saturation with both phases. Funicular liquid bodies touch each other and merge, forming a continuous network of both phases in the porous medium. The complete saturation regime refers to a porous medium that is completely saturated with one phase.

For a fluid phase in the pendular regime, the fluid is immobilized by capillary trapping. Whether a fluid phase will be trapped during immiscible-fluid flow depends on the pore geometry (size and spatial distribution) of the porous medium, the fluid and solid properties (viscosity, surface tension, and contact angle), the rate of fluid flow (or phase displacement), and the sequence of flow of a wetting and nonwetting phase (drainage vs imbibition). The simplest model of a porous medium is a bundle of capillary tubes in which each tube has a uniform diameter, but the diameter of the tubes may differ, giving a size distribution. Which fluid phase occupies which pore (or tube) diameter depends on the surface tension between the two fluid phases and the capillary pressure between the two fluid phases. The simplest relationship is given by Laplace's equation for a cylindrical tube,

$$r = -2\sigma(\cos\theta)/P_c,$$

where r is the radius of the tube, σ is the surface tension of the nonwetting phase, θ is the contact angle between the nonwetting fluid phase and the solid in the presence of the wetting phase, and P_c is the capillary pressure (the difference in pressure between wetting and nonwetting phases). The size of the pore diameter accessible to the nonwetting phase is inversely proportional to the capillary pressure.

For tubes with uniform diameters, trapping of the nonwetting phase does not occur (Chatzis et al 1983). However, when the cross-section of a single tube varies along its length so that the tube possesses pore bodies and pore throats, trapping of the nonwetting phase may or may not occur during displacement, depending on the aspect ratio of the variation in pore size (i.e. the ratio of the pore body size to the pore throat size) (Chatzis et al 1983). At relatively low aspect ratios, no trapping of a nonwetting phase occurs in the pores (Figure 2*a*). When the aspect ratio is high, trapping occurs in the pore bodies (Figure 2*b*).

The amount of trapped immobilized phase is generally quantified using residual saturation (Sn_r). Sn_r is defined as the ratio of the volume of the trapped phase (V_{trap}) to the volume of voids,

$$Sn_r = V_{trap}/V_{voids}.$$

According to the definition of residual saturation, funicular and complete saturation liquids are not included in Sn_r.

The trapping of a fluid phase around grain contacts such as occurs in the pendular regime can affect the mechanical properties of a porous medium such as

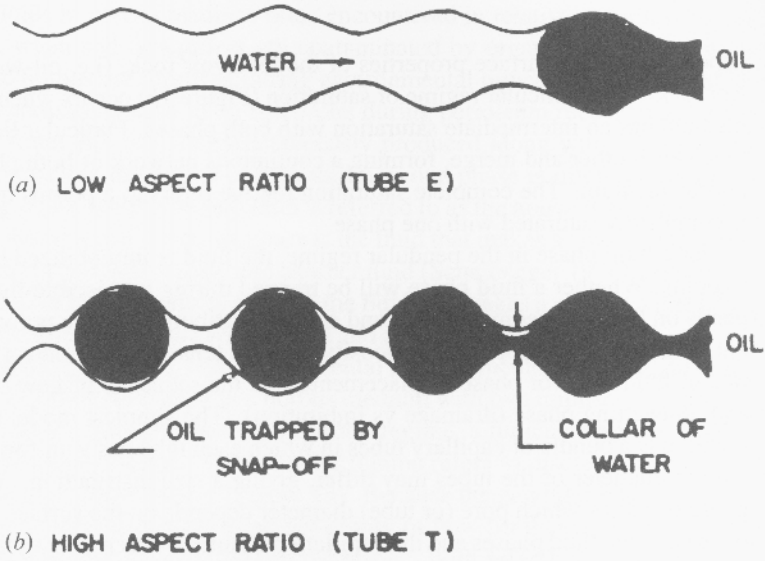

Figure 2 Effect of low (*a*) and high (*b*) aspect ratios on trapping in nonuniform capillaries (Chatzis et al 1983).

the Young's modulus. The stiffness of the grain contact will be greater with the presence of a pendular ring of liquid surrounding the grain contacts than in the presence of just air. The change in Young's modulus produced by pendular saturation will affect the velocity of seismic waves propagated through a porous medium. Seismic-wave attenuation can also be altered by the presence of pendular saturation if the stresses from a propagating seismic wave are sufficient to move the fluid-fluid interface. A change in the meniscus of the trapped fluid phase will alter the stiffness of the grain contact, which may explain frequency-dependent seismic attenuation (Moerig 1996). The literature review presented in the succeeding sections of this paper indicates that fluid around grain contacts greatly affects seismic-wave attenuation and velocity through either stiffening of grain contacts or local flow-attenuation mechanisms.

Flow conditions in porous media have a significant influence on immiscible-phase displacement and the resulting distribution of multiple fluid phases. For example, flow rate, direction of flow, and the sequence of flow of wetting and nonwetting phases make a direct contribution to phase displacement and entrapment. In two-phase flow, phase displacement is often referred to as either imbibition or drainage. For imbibition, the porous medium is initially saturated with a nonwetting fluid. The wetting fluid is imbibed into the sample by capillary forces, which results in the displacement of the nonwetting fluid from the pore space. For drainage, the porous medium is initially saturated with a wetting fluid. As the wetting fluid is drained from the porous medium, nonwetting fluid flows into the pores.

Cadoret et al (1995) used X-ray computerized tomography to visualize the fluid distribution within a rock during drainage and imbibition. They confirmed that the fluid distribution strongly depends on the saturation technique used. The imbibition process tends to create a homogeneous distribution of the two fluid phases, resulting in a saturation that is approximately constant at all locations. In contrast, the drainage process creates a more-heterogeneous saturation distribution, with fully saturated pores adjacent to partially saturated elements. Fluid-phase distribution plays a key role in the attenuation of seismic waves. The spatial distribution of multiple fluid phases can produce seismic-wave attenuation, which is attributed either to scattering from regions of nonuniform or varying saturation or to local or global flow between regions with partial saturation or regions that are unsaturated.

The spatial distribution of multiple phases in a porous medium is related to dynamic and static stresses. The capillary number, N_{ca}, is a measure of the ratio between the controlling dynamic stress, which tends to move the nonwetting phase, and static capillary stress, which manages to hold the nonwetting phase in place. The equation for the capillary number is

$$N_{ca} = v\mu/\sigma \cos\theta,$$

where v is the fluid velocity, μ is the dynamic viscosity, σ is the surface tension between the wetting and nonwetting phases, and θ is the contact angle of the liquid-solid system. Much research, mainly involving experimental investigation of the relationship between residual nonwetting-phase saturation and N_{ca}, has been

published (e.g. Ng et al 1978, Larson et al 1981, Morrow et al 1988, Pennell et al 1996, Zhong et al 2000). Among the different works, some general conclusions have been reached: Residual oil saturation, Sn_r, is independent of N_{ca} up to an N_{ca} of $\sim 2 \times 10^{-5}$, Sn_r decreases with N_{ca} over the range of roughly $2 \times 10^{-5} < N_{ca} < 2 \times 10^{-3}$, and all residual saturation is virtually mobilized with an N_{ca} of 5×10^{-3}.

The average length of a trapped blob (residual saturation) in the direction of flow is also a function of capillary number (Lenormand & Zarcone 1988, Mayer & Miller 1992, Zhong 1999). The blob length and size decrease with increasing N_{ca}. Chatzis et al (1984) reported that during initial stages of mobilization of residual oil, as the N_{ca} exceeds a critical value, oil blobs break up into smaller and shorter blobs, with a significant fraction being only temporarily mobilized. Related to the length and size reduction caused by increasing N_{ca}, the shape complexity (Figure 3) of trapped oil blobs also decreases with increasing N_{ca} (Zhong 1999). The geometry and spatial distribution of residual saturation within a porous medium will affect seismic-wave attenuation and velocity because the pore space is filled with multiple fluids that can respond differently to the passage of seismic waves. As we will see in the succeeding literature review, fluid viscosity plays an important role in seismic-wave velocity dispersion and attenuation.

The distribution of multiple fluid phases within a porous medium is also affected by the difference in density among the fluids during flow. When there is a difference in density between immiscible fluids, buoyancy plays a role in mobilizing and trapping fluid. Bond number, N_b, is usually used to include the influence of buoyancy in the analysis of fluid displacement and entrapment. The equation for the bond number is

$$N_b = g(\rho_n - \rho_w)r/\sigma \cos\theta,$$

where g is the acceleration due to gravity; ρ_n and ρ_w are the density of nonwetting and wetting phases, respectively; σ is the surface tension between the wetting and nonwetting phases; and θ is the contact angle of the liquid-solid system. Morrow & Songkran (1981) showed that for vertical displacement of a light nonwetting phase (oil) by a denser wetting phase, trapped oil saturation is inversely correlated with N_b. However, it was reported that when DNAPL was displaced by a less-dense aqueous phase, the DNAPL saturation increased with N_b for upward displacement (Dawson & Roberts 1997). It should be noted that if the downward mobilization of DNAPL is considered, residual saturation decreases with increasing buoyancy force. The role of buoyancy forces in seismic-wave attenuation mechanisms has been mostly ignored in theoretical models that study induced fluid flow caused by a propagating seismic wave. If the passage of a seismic wave induces fluid flow in a porous medium containing both hydrocarbons and water, buoyancy forces may mobilize the trapped less-dense phase, which will lead to frequency-dependent seismic-wave attenuation and velocity, as well as fluid saturation.

Modeling of wave propagation in porous media usually follows two paths by attempting to explain (*a*) how rock microstructure influences the seismic properties of

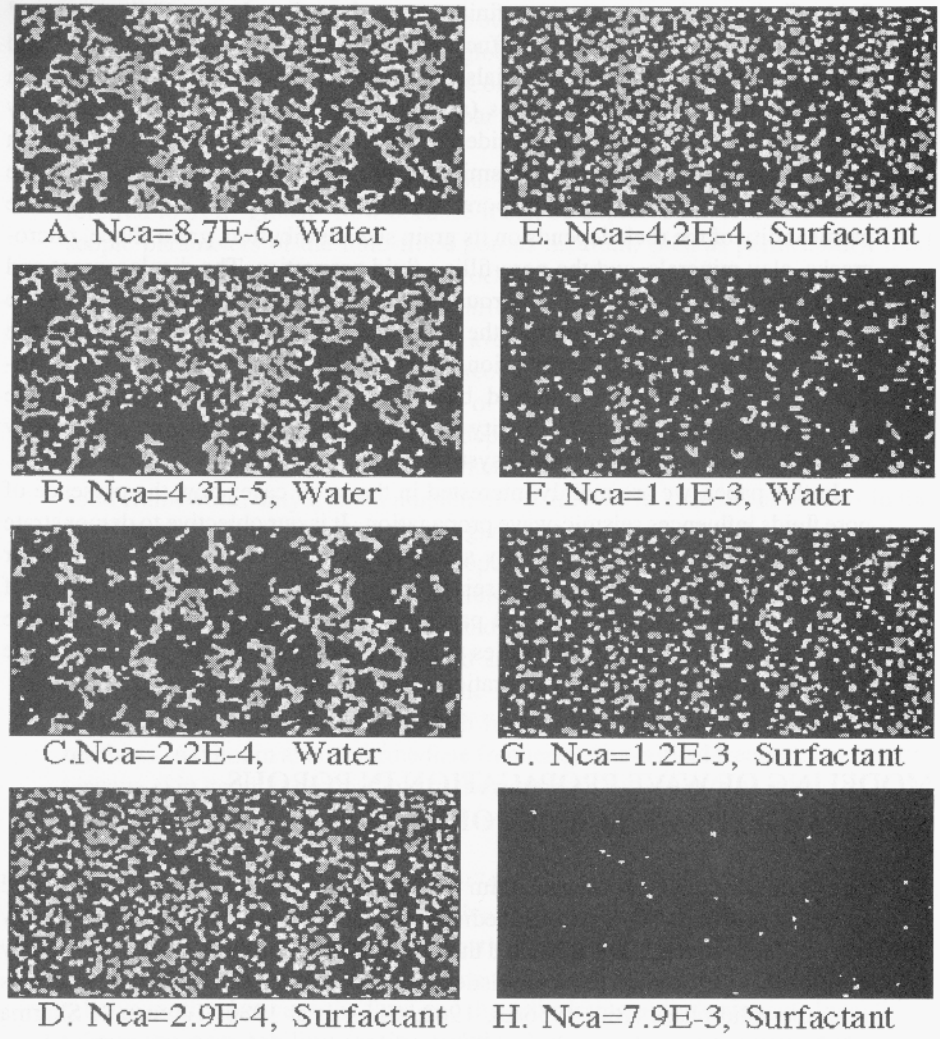

Figure 3 Images of NAPL blobs following mobilization as a function of capillary number and flood type. All images show the same region (3.8 cm by 6.1 cm) of the micromodel. NAPL and aqueous phase are represented by the white and black regions, respectively. Direction of flow is from left to right in images (Zhong 1999).

granular rocks at all frequency ranges and (*b*) how viscous fluid-flow and mineral-fluid interactions that take place on grain surfaces and at grain contacts influence the seismic properties.

On the grain scale, a porous medium (e.g. soil, sediment, or rock) can be characterized in terms of grains, cementing materials, clay minerals, and pore-filling

fluids. Grains are in contact over a finite area and cemented or partially cemented together, resulting in a contact stiffness that depends on the external stress and the properties of cementing materials. Pores are connected or isolated and can be filled with multiple fluid phases (air, gas, oil, organics, or water). Usually only interconnected pores are considered when working with fluid flow through a porous medium. However, for seismic-wave propagation through rock, both the connected pores and unconnected pores affect the elastic moduli of the rock. The permeability of the rock depends on its grain size distribution, grain shape, microcracks, clay minerals, and the pore-filling fluid properties. The displacement and entrapment of fluid phases in a porous medium are significantly affected by the properties of the fluids present in the system and the material properties of the porous medium (mineral composition, grain size, pore geometry, pore connectivity, etc). Residual saturation and blob size (trapped-phase dimensions) are functions of pore geometry, viscosity difference, interfacial tension, and density variations in the multiphase liquid system.

In this paper, we are mainly interested in the latter case: how the presence of pore fluids influences seismic-wave propagation. It is our objective to demonstrate that seismic delineation of partially saturated or unsaturated patches in rock or sediment can be performed using seismic waves. We present a brief review of wave propagation in saturated and partially saturated media followed by some recent experimental results of studies using acoustic tomography to delineate the spatial distribution of residual saturation in an unconsolidated porous medium.

MODELING OF WAVE PROPAGATION IN POROUS MEDIA AND THE EFFECT OF PORE FLUID

The permeability of a porous medium will affect the ability of multiple fluid-solid matrix interactions in the porous medium to occur at the same time. In laboratory and field experiments, it is observed that seismic-wave transmission is affected by the physical and chemical characteristics of the pore-filling fluid and its interactions with the solid phase (Biot 1956a,b, 1962; Clark et al 1980; Tutuncu & Sharma 1992). The exact mechanisms are still debated, and several mechanisms have been proposed to describe the change in seismic-wave attenuation and velocity with the type and extent of saturation of the pore. The proposed energy loss mechanisms for fluid-saturated porous media can be classified into three categories: (*a*) viscoelastic loss, (*b*) fluid-solid surface physicochemical interaction loss, and (*c*) scattering loss. Seismic-wave attenuation in saturated and partially saturated porous media is most likely caused by a combination of all three mechanisms, although in many instances one mechanism may dominate.

Viscoelastic Loss

Viscous and inertial coupling between the frame of a porous rock and its pore fluid can cause seismic-wave energy to be dissipated as heat within the liquid phase (Biot

1956a,b; Jones 1986) and hence cause attenuation of seismic waves. Viscous-loss models proposed to date include the global-flow theory of Biot (1956a,b) and the local-flow theories of Biot (1962), O'Connell & Budiansky (1977), Mavko & Nur (1979), Murphy et al (1986), and Akbar et al (1994).

Global-Flow Mechanism Traditionally, the Biot mechanism (Biot 1956a,b) is referred to as a "global" flow because it can be expressed in terms of the macroscopic parameters of the fluid-filled porous medium, such as permeability, fluid viscosity, and elastic constants of the rock. In the Biot theory there are two distinct interpenetrating effective media that affect seismic velocity and attenuation: the fluid phase and the solid phase. The average motions of both the solid and fluid phases are treated separately by the theory. Biot considered the effects of viscous losses caused by the relative motion of the pore fluid and the solid framework. At low frequencies, the viscous-skin depth is much greater than the pore size, and the solid and fluid phases move together. Because the pore fluid moves with the solid framework, only a small amount of seismic-wave dissipation occurs. In the low-frequency limit, the Biot theory gives expressions identical to those derived by Gassmann (1951). The elastic properties of the fluid-saturated frame can be calculated from the properties of the fluid and the dry frame. At high frequencies, the viscous-skin depth is very small and laminar-fluid flow breaks down. The inertia of the pore fluid causes the fluid and the solid frame to move out of phase and results in a small amount of seismic-wave dissipation per cycle. The net effect is that higher velocities occur at high frequencies. Biot showed that dissipation reaches a maximum at an intermediate frequency (the critical frequency) when the viscous-skin depth is comparable to the pore size: $\omega_c = \eta\phi/\kappa\rho_f$, where ω_c is the critical frequency, η is the viscosity, ϕ is the porosity, κ is the permeability, and ρ_f is the fluid density.

Stoll & Bryan (1970) and Stoll (1974, 1977) applied the Biot theory to the attenuation of seismic waves as a function of frequency in marine sediments. They included loss terms for the complex elastic parameters of the solid frame to take into account energy loss at grain-to-grain contacts as well as energy loss caused by the relative motion between the fluid and the solid frame of the sediment. In addition to porosity, permeability, density, and the elastic moduli for the fluid, frame, and matrix, the numerical model of Stoll & Bryan (1970) also requires two other free constants derived from the Biot theory, a pore size parameter and a structure constant that must be chosen or obtained from experiments. The structure constant is a function of the pore geometry (size and shape) as well as the interconnectivity or tortuosity of the pores. McCann & McCann (1985) incorporated the distribution of pore sizes into the Biot theory and presented a multi-pore-size model that provided physically reasonable values of shear and frame bulk moduli. Using a distribution of pore sizes in the Biot theory results in a linear increase in attenuation with increasing frequency for intermediate frequencies. Hamilton (1972) concluded that the majority of sediments exhibited seismic-wave attenuation that was a linear function of frequency for frequencies between 0.01 and 1.0 MHz. Yomamoto & Turgut (1988) presented mathematical expressions for the permeability and a

viscous correction factor to be used in the Biot theory for an arbitrary distribution of pore sizes. They found that the attenuation and velocity dispersion characteristics of these elastic waves through porous media become strongly dependent on the pore size distribution.

Local-Flow Mechanism Experimental investigations have demonstrated that in certain cases the Biot theory fails to adequately predict velocity dispersion and attenuation (O'Connell & Budiansky 1977, Mavko & Jizba 1991). The Biot theory predicts that increasing fluid viscosity shifts relaxation toward higher frequencies. This contradicts the observed experimental data, as noted by Jones & Nur (1983), Bulau et al (1984), and Winkler (1985). Winkler (1985) showed that increasing fluid viscosity in Berea sandstone shifts the relaxation toward lower frequencies. Akbar et al (1993) theoretically observed that the relaxation shifts toward lower frequencies as permeability decreases in Fontainebleau sandstones. Both experiments and models suggest that the cause is related to a "local" fluid mechanism; that is, when a porous medium is excited by a passing seismic wave, grain-scale heterogeneities (such as pore shape, orientation, and saturation) will produce a local pressure gradient that causes pore fluid to be squeezed from more-compliant to less-compliant regions. For example, a flat crack is mechanically weaker (or more compliant) than a round pore, so pore fluid will be squeezed from the crack into the pore. In a partially saturated porous medium, fluid will flow into empty regions of the pore space. The local-flow model is often referred to as the squirt-flow mechanism and has been investigated by examining fluid flow in individual cracks (Mavko & Nur 1979, Miksis 1988) as well as at grain contacts (Palmer & Traviolia 1980, Mavko & Jizba 1991). Attenuation and velocities have been calculated by considering viscous-energy losses or through a complex modulus (Murphy et al 1986). It is concluded that at low frequencies there will be sufficient time for the flow to occur. The fluid pressure will equilibrate, and the rock will be in a relaxed state. At high frequencies there will not be enough time for the flow to occur, and the rock will be in an unrelaxed state; in other words, the fluid does not move out of the contact regions between grains or stiffer regions of the porous medium. The porous medium is therefore stiffer at higher frequencies than at lower frequencies, and this results in higher wave velocities at high frequencies. At intermediate frequencies, the viscous interaction between fluid and solid will be a maximum and maximum attenuation will occur.

Within the past 10 years, attempts have been made to relate the squirt-flow mechanism to measurable properties of a porous medium for a range of frequencies. Dvorkin & Nur (1993) linked the frequency dependence of squirt-induced pressure in the soft cracks with the porosity and permeability of the soft-pore space and the characteristic squirt-flow length. They modeled seismic-velocity dispersion and attenuation in fully saturated rocks by employing the squirt-flow mechanism. The theoretical predictions were matched with the experimental measurements of attenuation or velocity. Akbar et al (1993) related the squirt mechanism to

permeability by using a solution based on simplified pore geometry (needlelike pores). In another paper, Akbar et al (1994) used the squirt-flow mechanism to relate the effective dynamic-bulk modulus of a rock to macroscale parameters such as permeability, porosity, dry-bulk modulus, and fluid and gas properties. They investigated the influence of the fluid distribution on the viscoelastic behavior of a porous material on both local and global scales and proposed a macroscopic (global) squirt-flow mechanism that refers to flow between fully saturated "patches" that are much larger than the grain size and unsaturated patches when the saturation is partial or not uniform. In their model, the macroscopic squirt mechanism dominates at low frequencies (0.001–1 Hz), whereas at higher frequencies the fluid is macroscopically unrelaxed (trapped in stiff portions of the rock) and the system behaves as if it is uniformly saturated on a macroscale. The microscopic squirt mechanisms dominate at high frequencies (10 Hz–10 kHz) and result in another peak in the attenuation curve as a function of frequency (Figure 4). The characteristic frequencies of the local squirt flow and global squirt flow depend on the scale of the fluid distribution, frequency, and saturation as well as the fluid and gas properties and the macroscopic properties of the rock, such as porosity, permeability, and dry-bulk modulus. Dvorkin & Nur (1993) combined the Biot flow and local

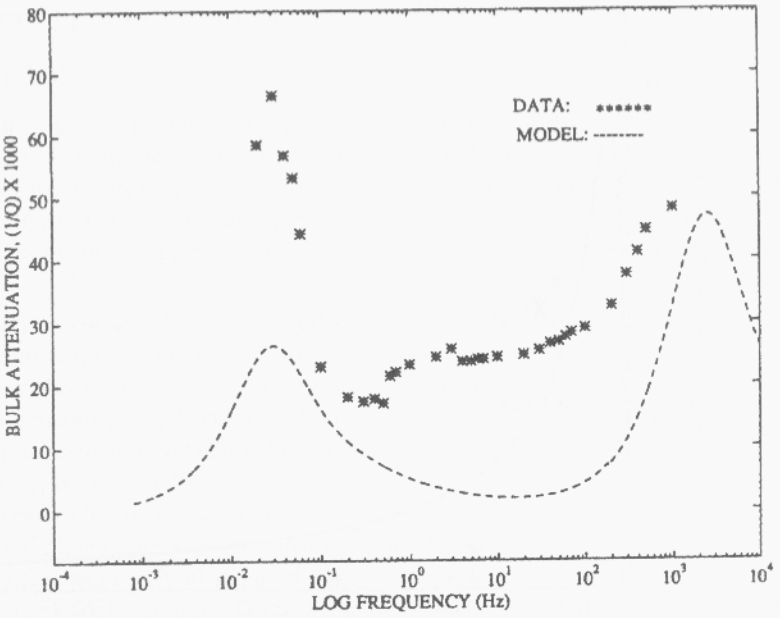

Figure 4 Bulk attenuation as a function of frequency for quartzite. The dashed line is the theoretical prediction by the local and global squirt-flow theory (Akbar et al 1994); the asterisks are the data measured by Paffenholz & Burkhardt (1989). (From Akbar et al 1994.)

(squirt)-flow mechanism for partially saturated rocks. They hypothesized that because both mechanisms may operate in a porous rock simultaneously, these two modes of solid-fluid interaction will affect each other via fluid mass balance. The integrated model (the Biot and squirt-flow model) gives more-realistic estimations of seismic-wave attenuation and velocity dispersion as functions of measurable parameters such as frequency, porosity, permeability, and fluid viscosity (Figure 5).

Physicochemical Interaction between Fluid and Solid

Murphy et al (1984) developed a model predicting the frame bulk modulus reduction in sedimentary rock as a function of fluid chemistry and effective pressure based on contact theory (contacts between grains) and surface chemistry. They showed that at low pressure the stiffness of contact decreases with decreasing surface energy. The adsorption of different chemicals (*n*-hexane, benzene, methanol, and water) onto quartz surfaces lowered the surface energy, which weakened the contact stiffness and thus reduced the frame bulk moduli. The reduced frame bulk moduli increased seismic-wave attenuation. Their model showed qualitative agreement (Figure 6) with the experimental data of Clark et al (1980).

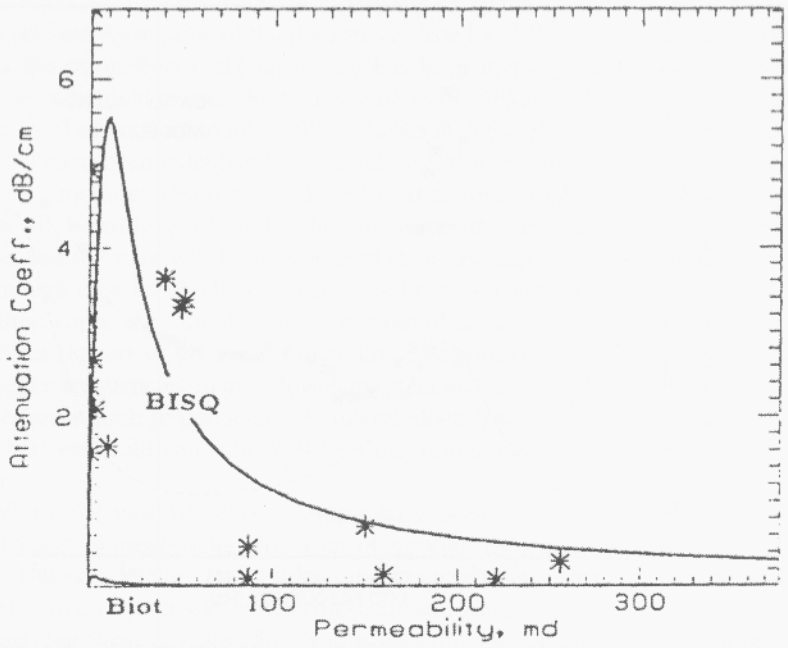

Figure 5 Attenuation coefficient vs permeability from the Biot and squirt-flow theory (upper curve) and from the original Biot theory (lower). The asterisks are the experimental data from Klimentos & McCann (1990). (From Dvorkin & Nur 1993.)

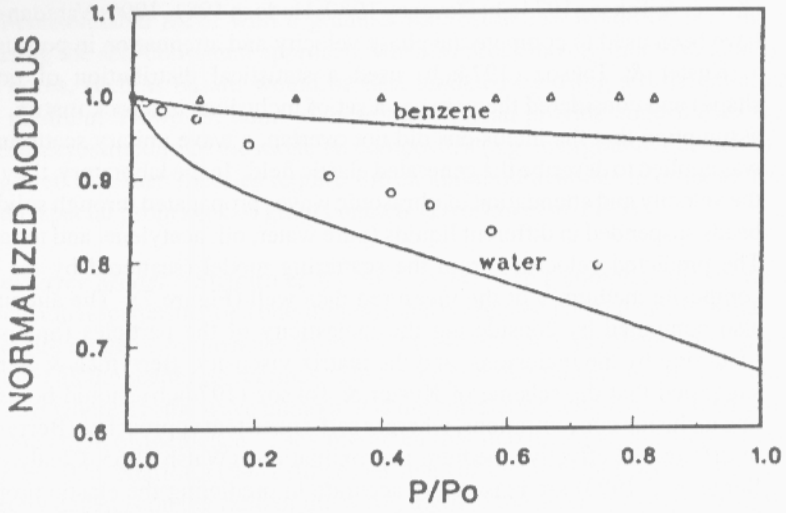

Figure 6 Normalized contact stiffness vs partial pressure as a function of fluid chemistry for benzene and water from the surface energy reduction theory (Murphy et al 1984). The measured data (circles and triangles) are for Coconini sandstone and are from Clark et al (1980). (From Murphy et al 1984.)

Scattering Loss

For dry rocks, attenuation mechanisms primarily result from scattering (Winkler 1983, 1985). In rocks fully or partially saturated with pore fluids, seismic waves scatter from pores and immiscible-fluid interfaces (Geller & Myer 1995, Seifert et al 1998). The next sections present a review of attenuation caused by scattering from inclusions and thin layers.

Inclusion Model For wavelengths that are long relative to pore sizes, a porous medium can be approximated by an equivalent homogeneous medium with effective elastic coefficients. Theoretical formulations for the elastic moduli of a homogeneous or multiphase medium with inclusions have been studied by a number of investigators (Hashin 1962; Walsh 1965, 1969; Wu 1966; Kuster & Toksoz 1974a,b; Berryman 1980).

In early classical averaging schemes (Voigt 1910, Reuss 1929, Gassmann 1951, Hill 1952), the pore geometry is not taken into account directly; only the physical properties and concentrations of components are used to predict effective elastic properties of the complete porous medium. Later models make a simplified assumption of the microstructure of granular porous media. The porous medium is idealized as a homogeneous background hosting isolated inclusions with simple geometric shapes (spherical, elliptical, and crack shaped), or the host medium is also considered to be a composite. Single- or multiple-scattering-wave theories

(Kuster & Toksoz 1974a,b; Devaney 1980; Hudson 1981, 1990; Varadan et al 1989) have been used to compute the phase velocity and attenuation in porous media.

Kuster & Toksoz (1974a,b) used a statistical distribution of pores (pore shape) and considered the pores as a set of inclusions in a rock matrix. Under the assumption that the inclusions did not overlap, a wave unitary scattering method was applied to describe the generated elastic field. In the laboratory, they measured the velocity and attenuation of ultrasonic waves propagated through solid spherical beads suspended in different liquids (pure water, oil, acetylene, and tetrabromide). The predicted velocities from the scattering model (scattered by the "effective composite medium") fit the measured data well (Figure 7). The attenuation was also computed by considering the inelasticity of the particles (inclusions), the scattering by the inclusions, and the matrix viscosity. Berryman & Berge (1996) suggested that the scheme of Kuster & Toksoz (1974a,b) should be used for dilute inclusion concentrations, whereas self-consistent approaches (Berryman 1980) or differential effective medium approximations (Walsh 1965, Clealy et al 1980, Berge et al 1993) are reasonably accurate in predicting the elastic properties for high inclusion concentrations. Different sediments or rocks should be modeled by different models to obtain the best result (Berge et al 1993, 1995). For example,

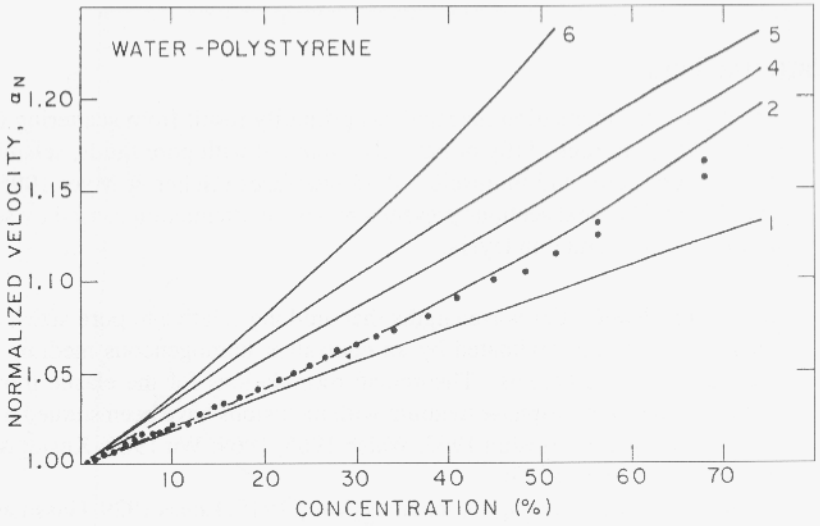

Figure 7 Normalized effective velocity vs volume concentration of inclusions for a water-polystyrene suspension. Normalized velocity is the ratio of the observed velocity to the velocity of pure matrix material (water in this case). Experimental data are shown by solid circles. The numbers next to the theoretical curve indicate the model numbers: 1, the model of Mal & Knopoff (1967); 2, the model of Kuster & Toksoz (1974); 3, the Reuss (1929) average; 4, the Hill (1952) average; 5, the Voiget (1910) average; and 6, the time average model (Kuster & Toksoz 1974).

well-consolidated rocks with a granular microstructure would be best modeled by using the self-consistent approach, whereas rocks having more-isolated cracks and pores, such as basalt, would be best modeled by using a differential effective medium. However, none of these theories can provide control over the detailed microstructure of the modeled composites (e.g. intergranular cements). It is suggested that such theories require substantial modifications in order to account for the special properties of grain contacts (Dvorkin et al 1999).

Thin-Layer Model Shapiro et al (1993, 1994) gave a complete theory for one-dimensional scattering for a one-dimensional correlated layered medium that spans the entire range of frequencies from effective-medium to ray theory and therefore includes all the scattering regimes. Their theory shows that attenuation depends on $kd \cos\theta$ where k is the wave number, d is the correlation length of the medium, and θ is the angle of incidence. They predicted that maximum attenuation will occur at $kd = 0.5$. Marion (1994) suggested that for uncorrelated layers, the seismic velocity depends on the ratio of the wavelength to the layer thickness. Seifert et al (1998) conducted laboratory and numerical studies using the theory of Shapiro et al (1994) to study the mechanisms of P-wave transmission through NAPL-water-sand systems. In one dimension, the three-phase system is approximated by interleaved thin layers of different thickness, each composed of a single phase. The results show that P-wave scattering can explain the main features of the P-wave velocity and attenuation in unconsolidated porous media partially or fully saturated with two immiscible fluids (Figure 8*a*,*b*). This represents an alternative explanation to the theories that describe local fluid flow as the dominant mechanism for seismic-wave attenuation and velocity dispersion.

EFFECT OF PORE FLUID ON SEISMIC-WAVE PROPAGATION

Viscosity

The effect of fluid viscosity on seismic-wave attenuation and velocity is complicated because the seismic response is frequency dependent. Experiments (Wyllie et al 1962, Nur & Simmons 1969, Batzle et al 1999) have been performed on rock saturated with glycerol, whose viscosity depends on the temperature. Thus, by varying the temperature of the saturated sample, the effect of viscosity on seismic-wave velocity and relative attenuation can be measured. Nur & Simmons (1969) have shown that viscosity produces frequency-dependent seismic behavior. Gordon (1974) made a similar observation for water-saturated crystalline rocks. Dvorkin & Nur (1993) theoretically calculated the seismic velocity for a rock as a function of fluid viscosity by using the unified Biot and squirt-flow model. They observed that velocity dispersion increased with increasing fluid viscosity (Figure 9). Batzle et al (1999) measured S- and P-wave velocity of Upper Fox Hill sandstone

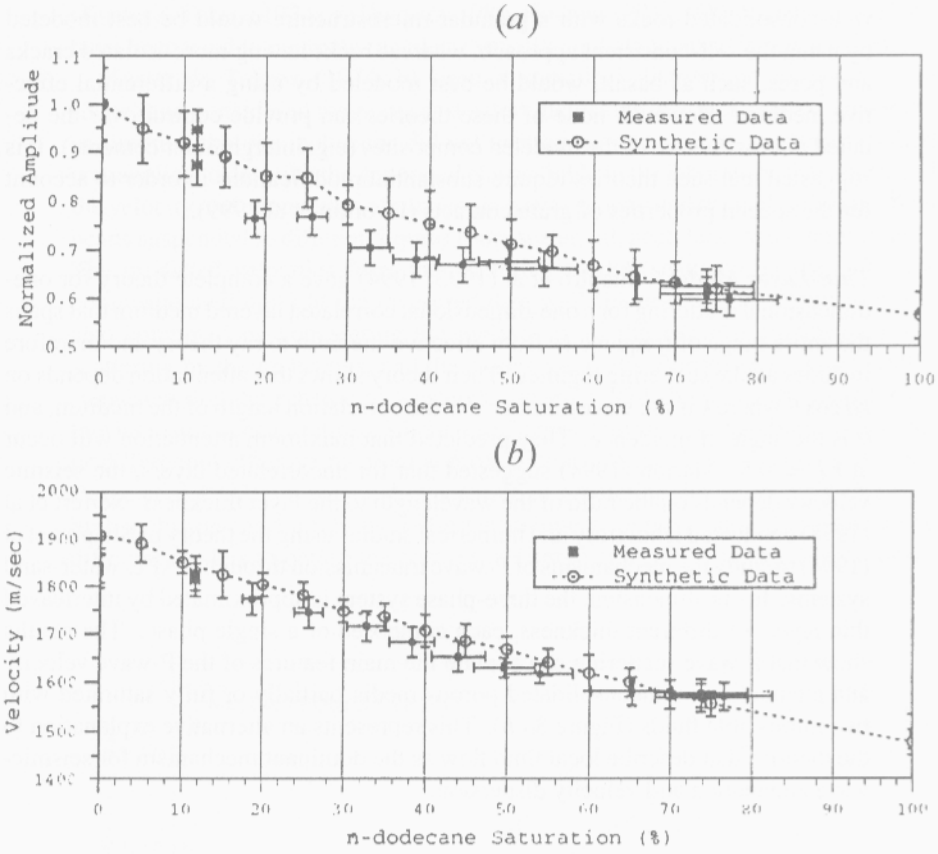

Figure 8 P-wave velocity (*a*) and normalized amplitude (*b*) as a function of *n*-dodecane saturation. Measured data are represented by squares, and the theoretical predictions from thin-layer scattering theory are represented by open circles. (From Seifert et al 1998.)

for both dry and glycerin-saturated conditions at 22 and 63°C (Figure 10*a*,*b*). The results showed that both shear and compressional wave velocities exhibited little frequency or temperature dependence in dry conditions. However, when the sample was saturated with glycerol, the sample exhibited strong velocity dispersion.

Surface Chemistry

Several investigations have been performed to examine how fluid properties affect fluid-grain interactions, thereby affecting acoustic-wave attenuation. Experimental studies have shown that a small amount of water can dramatically affect seismic-wave attenuation (Clark et al 1980, Tittman et al 1980, Cadoret et al

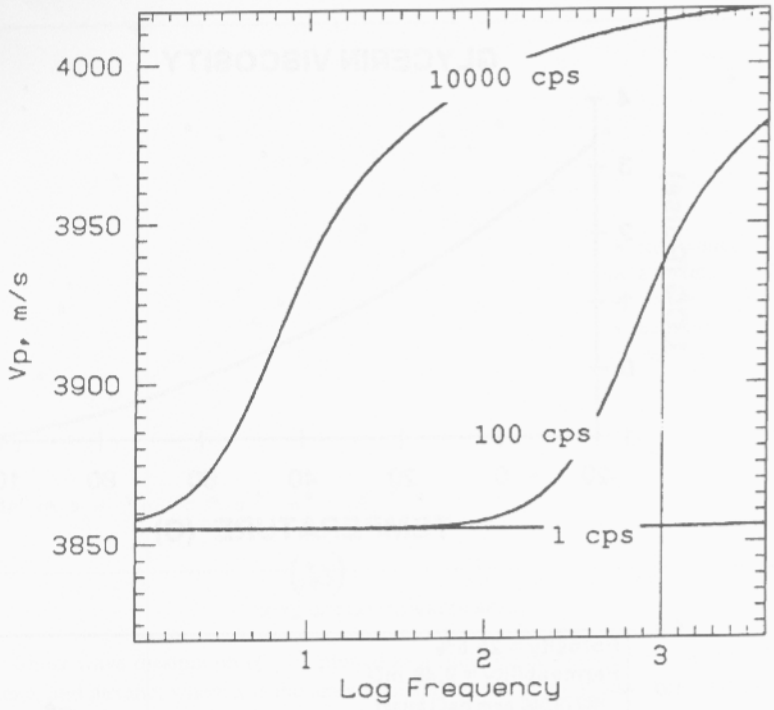

Figure 9 The effect of viscosity predicted by the Biot and squirt-flow model: compressional velocity V_p [meters per second (m/s)] vs frequency (Herz) for viscosities of 10,000, 100, and 1 centipoise (cps). (From Dvorkin & Nur 1993.)

1998). Clark et al measured the attenuation and velocity of several sandstones and limestones as a function of adsorbed-water mass. The results showed that shear-wave attenuation increased very sharply during the initial adsorption of water. They hypothesized that the initial monolayer or two of adsorbed water vapors will be closely bonded to the mineral surface and will contribute to the dissipation of seismic energy. Tests were also performed by Tittmann et al (1980) to study the relationship between type of volatile fluid and seismic-wave attenuation. The conclusion was that the dipole moment per unit molecular volume is the most important parameter affecting wave attenuation in rocks that contain a small amount of adsorbed volatile fluid. The polar nature and small molecular sizes of water and alcohol lead to greater volatile-fluid adsorption; stronger bonds, which decrease surface energy; and more attenuation. Benzene and hexane are not polar molecules and thus have no effect on wave attenuation (Figure 11).

Moerig (1996) studied an artificial sample consisting of wedge-shaped cracks made from glass. They found that adsorbed water vapor had no effect on wave attenuation or the stiffness of the artificial sample. Instead, they suggested that

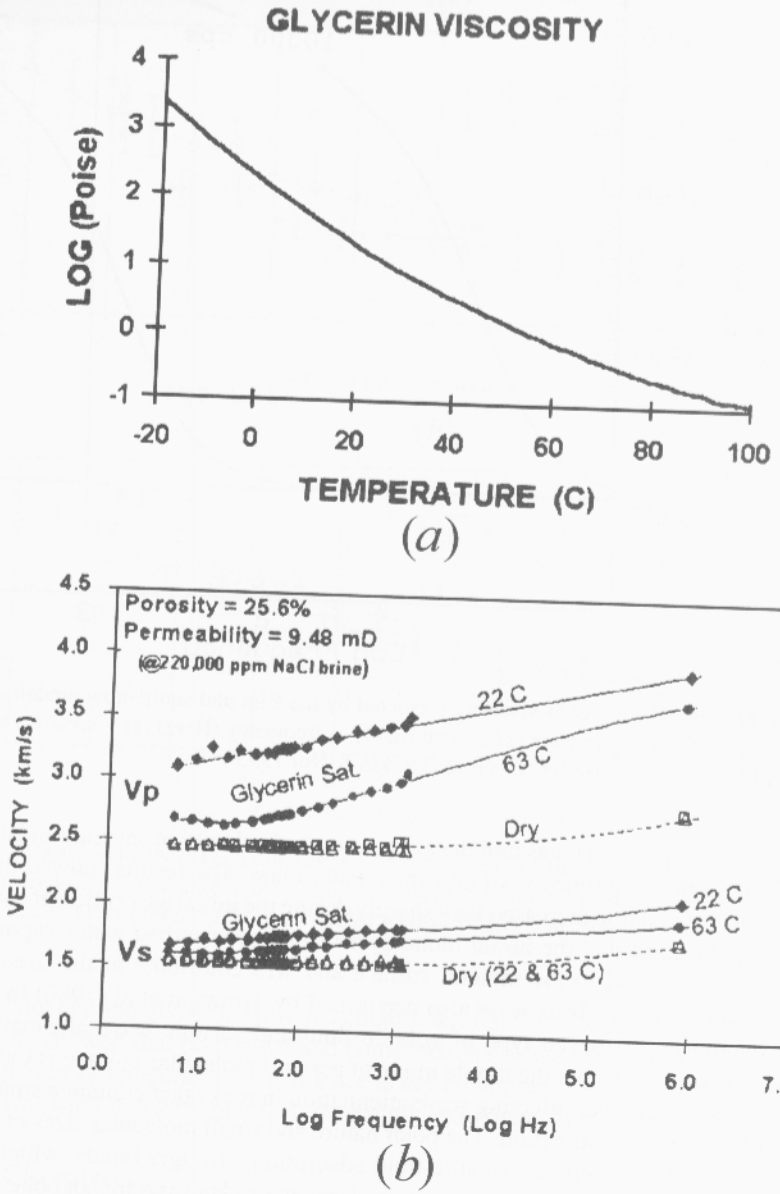

Figure 10 (*a*) Glycerin viscosity as a function of temperature; (*b*) compressional and shear velocity vs frequency for dry (open symbols) and glycerin-saturated (closed symbols) Upper Fox Hill sandstone. Velocities were measured at 22 and 63°C at an effective pressure of 17.24 MPa. (From Batzle et al 1999.)

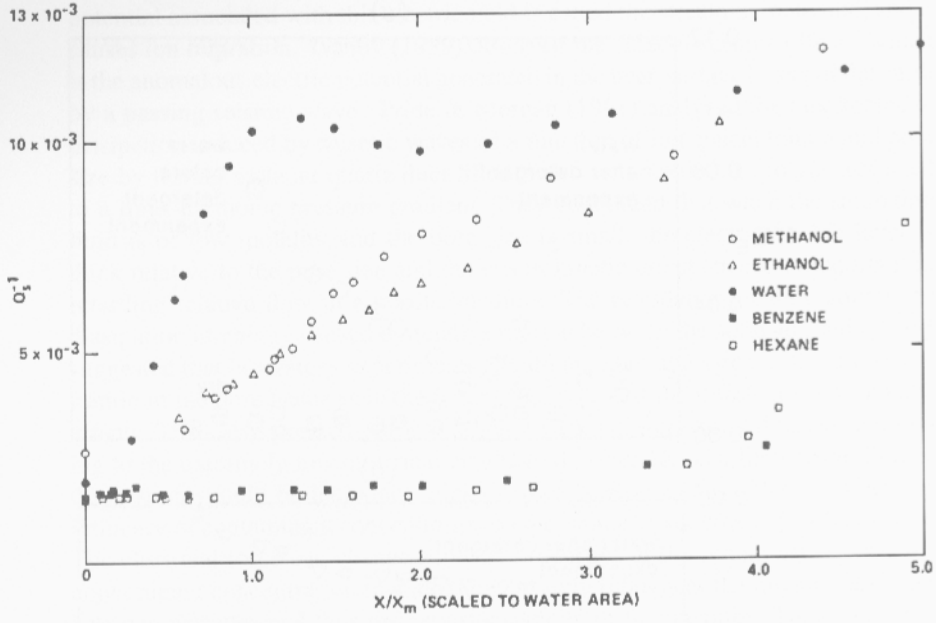

Figure 11 Shear wave dissipation (Q_s^{-1}) plotted as a function of x/xm for methanol, ethanol, water, benzene, and hexane, where x is the amount adsorbed per gram of adsorbent and xm is the amount necessary to form a monolayer. (From Tittmann et al 1980.)

surface wettability is an important factor that affects the stiffness of grain-to-grain contacts and the attenuation of seismic waves in the sample. After exposure to a detergent (or methanol, propanol, or acetone), the glass surface was contaminated with carbon-based molecules. This caused the surface to change from hydrophilic to hydrophobic, which altered the pattern of flow and changed the frequency dependence of the attenuation (Figure 12*a*,*b*). They also observed that a meniscus of a high-surface-tension fluid acts like a membrane that can stiffen the sample by adhering to the solid surfaces. The addition of a detergent to water reduces the surface tension. The reduction in surface tension reduced the stiffness and increased the attenuation.

Understanding the effect of surface tension and the resulting meniscus on seismic-wave attenuation and velocity is important for seismic monitoring of tertiary oil recovery or contaminant remediation. Light NAPL spilled in a vadose zone can form lenses in the capillary fringe above the water table. Schroth et al (1995) found that the LNAPL-water interfacial tension was a function of NAPL-water contact time (10% change in 1.5–6 h). On the basis of the work of Moerig (1996), this suggests that seismic measurements could be used to monitor changes in the fluid-solid-fluid interaction in the vadose zone.

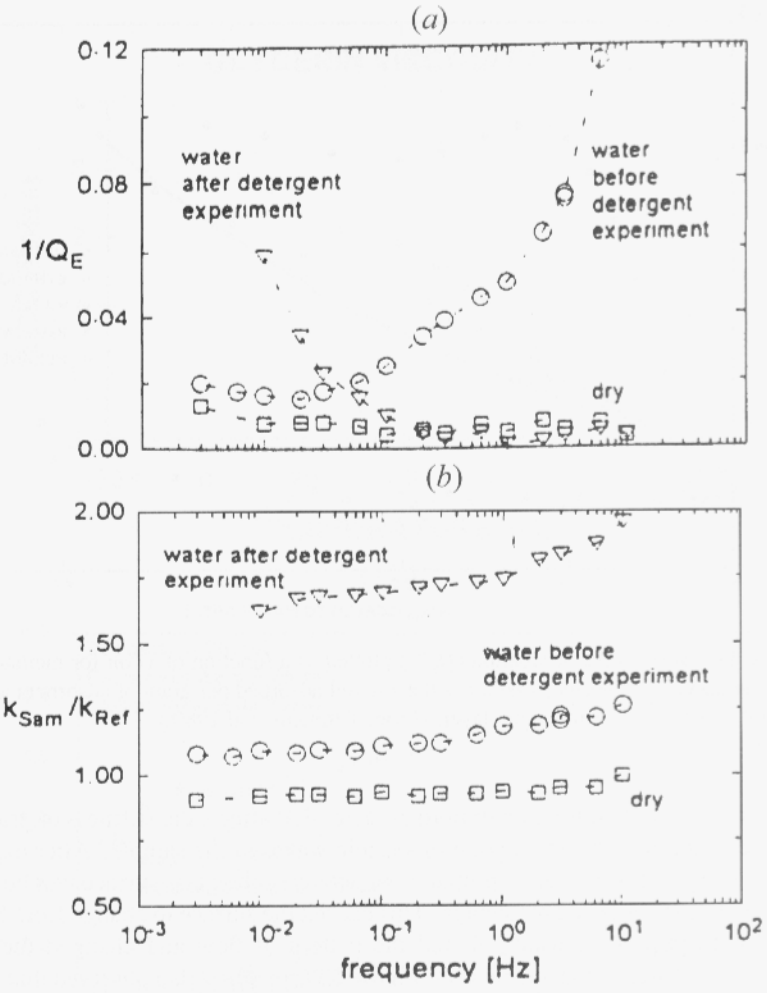

Figure 12 Attenuation ($1/Q_E$) and stiffness ratio (K_{sam}/K_{ref}) of a dry and partially water- and water/detergent-saturated sample. (From Moerig 1996.)

Ion Concentration

In an aqueous system, the fine particles of sediment carry charge on the surface and create a "diffuse double layer" around the particle. The first layer of cations is attached to the surface of the particle, and the second layer consists of a distributed charge around the particles. This arrangement produces a net charge that is strongest at the bond layer and decreases exponentially with distance from the particle. When the electrolyte in the fluid moves relative to a solid during seismic-wave propagation, an electric field is generated and energy is dissipated. The

potential associated with this electric field is called the streaming potential, and it causes ion migration. Ivanov (1939) observed the "electroseismic effect," which is the anomalous electric potential generated in the near-surface layers of the earth by a passing seismic wave. Pride & Morgan (1991) analyzed the electrokinetic dissipation induced by seismic waves as a function of ion concentration and pore size by testing a planar quartz duct filled with a symmetric electrolyte subjected to a time–harmonic pressure gradient. They concluded that when the saturating fluid is of low molality and the pore size is small, the electric double layer is thick relative to the pore size and the electrokinetic effects become important in retarding relative flow in a porous medium. The retardation of flow affects the dissipation of energy caused by relative motion between the solid and fluid. They suggested that laboratory experiments should maintain the same order of concentration in the pore water as in the in situ rock to avoid the different electrokinetic effects. They also pointed out that when a rock is saturated with crude oil, owing to the extremely low electrical conductivity of crude oils, high electrokinetic dissipation should be included. Elektorowicz & Konyukhov (1995) studied the influence of contaminant concentration on the acoustic properties of soft sediment. The electrical force can change acoustic properties of the sediments because the contaminant concentration in a medium strongly influences the interaction forces between particles and thus the acoustoelasticity of the medium. They combined previous work (Galvez 1989, Pride & Morgan 1991) on the streaming potential vs the heavy-metal concentration in the sediments and the potential's effects on sound attenuation to propose a new tool for using surface wave modulation to study the dynamic properties of the uppermost layer of soft sediments.

Li & Pyrak-Nolte (1998) reported that compressional-wave amplitudes increase and then decrease as a function of the ion exchanges between grains and pore water. They calculated both van der Waals potential and electrostatic repulsive potential between sediment grains and suggested that when the total ion concentration in the pore water reached a minimum, the electric double-layer repulsive force exhibited a maximum value, which produced a maximum reduction in the contact stiffness (Figure 13*a*,*b*).

Saturation Conditions

Theoretical and experimental studies of various gas, water, and oil saturations (Bacri & Salin 1986, Knight & Nolen-Hoeksema 1990, Cadoret et al 1995, Geller & Myer 1995, Knight et al 1998) have shown that the relationship between fluid saturation and both seismic-wave velocity and attenuation is complicated because the spatial distribution of fluid in the rock affects the viscoelastic response of a porous material (Biot 1956a,b; O'Connell & Budiansky 1977; Akbar et al 1994). In addition, the size (relative to wavelength) of heterogeneity in the rock induced by immiscible fluids plays an important role in seismic wave propagation (Geller & Myer 1995, Cadoret et al 1995). Many factors (i.e. pore structure and distribution, fluid properties, flow rate, and saturation history) have an impact on fluid distribution.

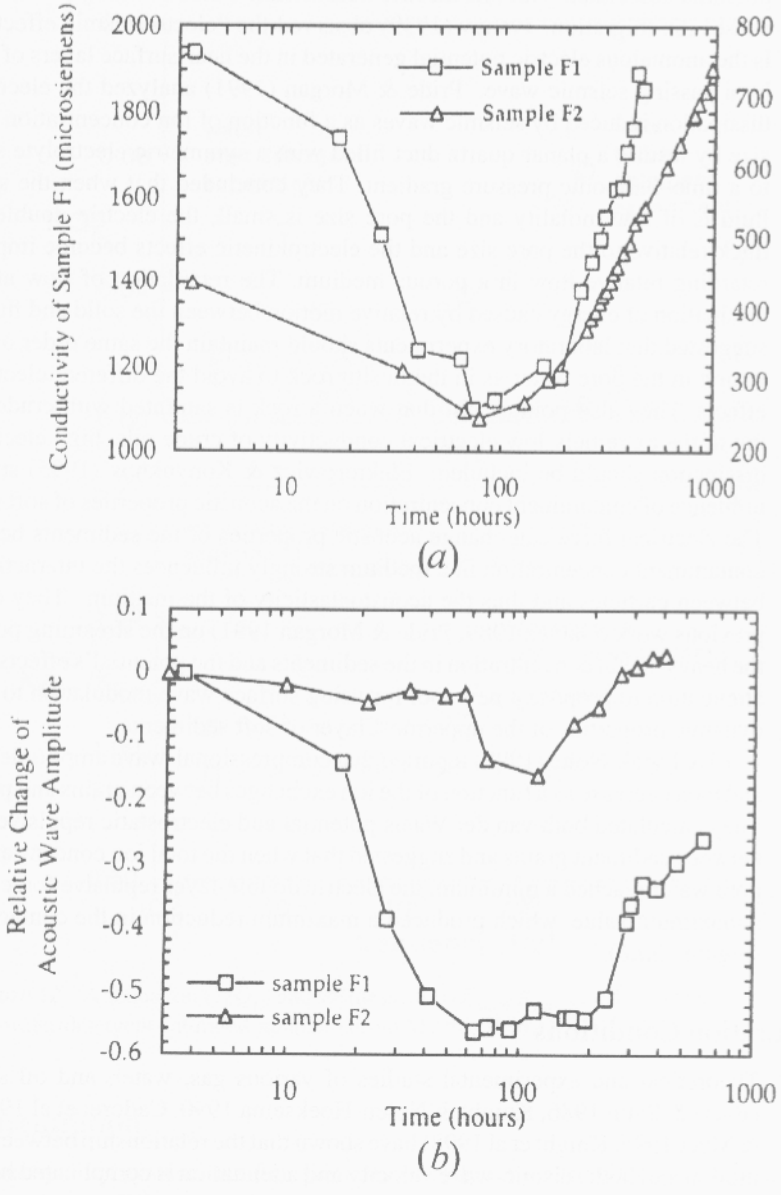

Figure 13 (*a*) Relative change in the peak-peak acoustic-wave amplitude as a function of time for two samples of water-saturated synthetic sediments (F1 and F2). (*b*) Pore water electrical conductivity as a function of time for samples F1 and F2. The data show that the compressional-wave amplitudes increase and decrease relative to the ions exchanges between grains and pore water. (From Li & Pyrak-Nolte 1998.)

For example, reservoirs with heterogeneous permeability distributions most often develop large gas- or liquid-saturated pockets (Akbar et al 1994).

Mechanisms for velocity dispersion and seismic-wave attenuation are usually based on a combined effect of scattering and intrinsic attenuation. Geller & Myer (1995) measured compressional-wave velocity and normalized amplitude as a function of NAPL saturation in initially water-saturated synthetic sediment composed of glass beads. They used *n*-dodecane, iso-octane, and freon for the NAPL. The results showed that both velocity and amplitude decrease with increasing NAPL saturation. However, the magnitude of the decrease in amplitude differed for each NAPL. Seifert et al (1998) related these results to the flow instability and viscous-fingering phenomena produced by the displacement of a more-viscous fluid by a less-viscous fluid in a homogeneous porous medium. They photographed the displacement of water by NAPL in a thin, glass-walled sandbox. The results showed that *n*-dodecane (which is more viscous than water) had a stable fluid front that migrated downward, whereas iso-octane (which is less viscous than water) exhibited fingering with large residual pockets of water. The viscous fingers caused stronger wave scattering, which may explain the measured data of Geller & Myer (1995).

Several experiments have been conducted on the saturation processes and the seismic responses of different rocks (Bacri & Salin 1986, Knight & Nolen-Hoeksema 1990, Cadoret et al 1995). In general, it was found that during drainage [i.e. injection of nonwetting fluid (gas or oil) in rock fully saturated with wetting fluid (water)] a linear decrease in compressional-wave velocity with increasing fluid saturation occurred over a wide range of saturation. This behavior differed dramatically from the change in compressional-wave velocity that occurred during imbibition, where only at saturations very close to 100% does velocity show a very steep increase (Figure 14).

Bacri & Salin (1986) reported measurements of the velocity variations in French Vosgian sandstone saturated with both oil and water, at different concentrations, from imbibition and drainage processes. They used an extension of the Biot-Gassmann theory for porous media saturated with two immiscible fluids. During the drainage process, the wetting fluid is linked to the grain contacts. As a result, the elastic moduli of the frame are assumed to be the moduli associated with the wetting fluid in contact with the frame, and the fluid is considered an effective mixture of oil and brine (wetting and nonwetting fluids). Using this Biot-Gassmann theory, they computed the velocity of sound at different levels of brine saturation that quantitatively matched the measured data. However, during imbibition, when wetting fluid is injected into the rock, only a portion of the wetting fluid is in contact with the grain contacts; the other portions of the wetting fluid are dispersed as pockets in the nonwetting fluid. In order to apply the Gassmann theory, more knowledge of the topology of oil and water (or nonwetting and wetting phases) around grain contacts is required.

The topology of residual phase distribution around a grain contact depends on the pore structure, pore size and distribution, surface property of pores, etc, all

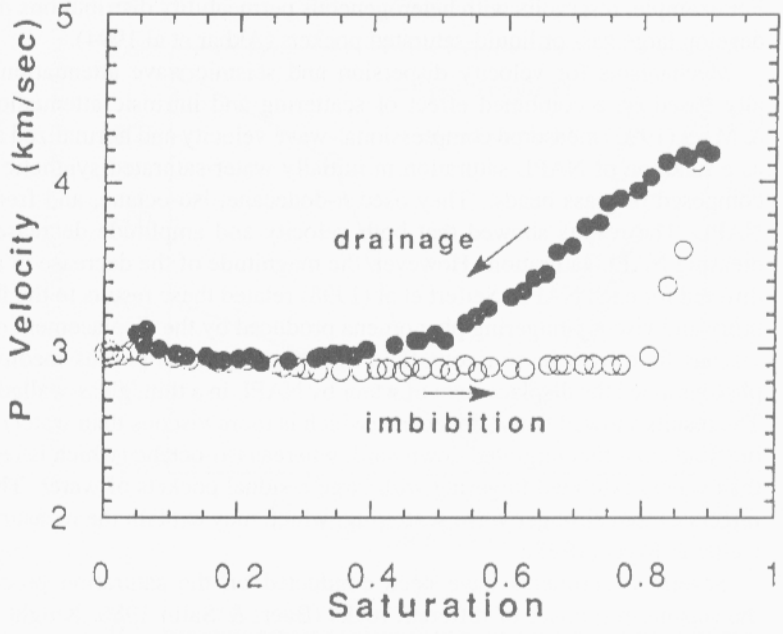

Figure 14 P-wave velocity vs saturation showing nonunique dependence on saturation in a tight sandstone. Open circles correspond to increasing saturation by imbibition, and closed circles correspond to decreasing saturation during drainage. (From Mavko & Nolen-Hoeksema 1994, based on Knight & Nolen-Hoeksema 1990.)

of which affect nonwetting-phase displacement and entrapment. The influence of particle size, which is expected to be related to pore size, on residual saturation was analyzed experimentally by Wilson & Conrad (1984). It was found that, in unsaturated media (three fluid phases), residual saturation increased with decreasing particle diameter. However, experiments conducted with saturated media (two fluid phases) show no influence on residual saturation by particle size. Wilson & Conrad (1984) found a higher Sn_r in sandstones than in glass beads. The higher Sn_r in sandstone was attributed to the smaller pore throats and lower degree of connectivity associated with the lower porosity (ϕ) ($\phi = 20\%$ for sandstone and 38% for glass beads). Hoag & Marley (1986) also studied the impact of particle size on Sn_r. They reported that when porous media went from being dry to being partially saturated, a more significant reduction of the Sn_r occurred in coarse sands than in finer sands. The Sn_r ranged from 14–55% in initially dry, coarse, and fine sands, respectively. They concluded that particle grain and pore size were of primary importance in controlling the Sn_r.

For unconsolidated uniform porous media, particle size (grain size) is directly related to permeability and determines how easily fluid can pass through the medium. Particle/pore size and spatial distribution also affect the trapped blob

(residual saturation) size distribution. The effect of pore geometry (aspect ratios) on seismic-wave propagation through partially saturated porous media has been studied by several investigators to determine the effect of partial saturation on the local-flow attenuation mechanism. Aspect ratio has an important influence on oil retention (Chatzis et al 1983); for example, the fraction of oil trapped in single pore bodies increases when the aspect ratio increases. Endres & Knight (1991) explored the effect of pore aspect ratio on seismic-wave velocity of different distributions of fluids in the pore space—a mixture of gas and liquid in all of the pores. They assumed ellipsoidal pores with a range of aspect ratios with thin cracks being compliant and round pores being stiff. Their results show that at high frequencies the rock is stiffer in both bulk and shear modes when liquid occupies the compliant cracks and that the rock is more compliant when there is gas in the compliant cracks. Mavko & Nolen-Hoeksema (1994) modeled the effects of different fluid distributions in a pore space with a distribution of compliances. They extracted information about the compliance of cracks at low confining pressures from high-pressure velocity data and used dry-rock data to predict the range of behaviors when pore fluids are introduced by using squirt theory. Their results suggest that two scales of saturation are important: the pore scale and the scale of saturated and unsaturated patches or regions of the porous medium (Figure 15). Akbar et al (1994) investigated the influence of the fluid distribution on the viscoelastic behavior of a porous material on both local and global scales by employing the squirt-flow mechanism. They found that when fluid distribution is nonuniform, two mechanisms contribute to attenuation. The macroscopic squirt dominates at low frequencies, and the microscopic squirt dominates at higher frequencies. Their model showed a quantitatively good fit to the measured data of both drainage and imbibition processes (Figure 16).

Knight et al (1998) showed that, under conditions of capillary equilibrium, different lithologies within a reservoir can have different saturations (patchy saturation), depending on the porosities and permeability (Figure 15). The heterogeneity in fluid distribution at the pore scale and the macroscale introduces a frequency-dependent stiffening of compliant regions. At the microscale, the pore fluid accumulated in thin compliant pores can flow freely into the dry pore space (the squirt-flow effect) at low frequencies. However, at high frequencies, the pressure equilibration does not take place. Pore fluid located in the thin compliant pores is therefore "locked." The fluid reinforces the compliant pores and thus acts to increase acoustic velocity. At the macroscale, at low frequencies, pore fluid can flow easily between a saturated patch and the neighboring undersaturated patch. Thus, the saturated patch is drained (or partially drained) in response to the passing wave. At sufficiently high frequencies, pore fluid is trapped in the saturated patch and the apparent stiffness of the patch becomes that of a fully saturated infinite rock region. Therefore, if pore fluid is arranged in patches, the apparent stiffening of partially saturated rock in response to a sound wave may take place even at low frequencies because of macroscale variation in the saturation.

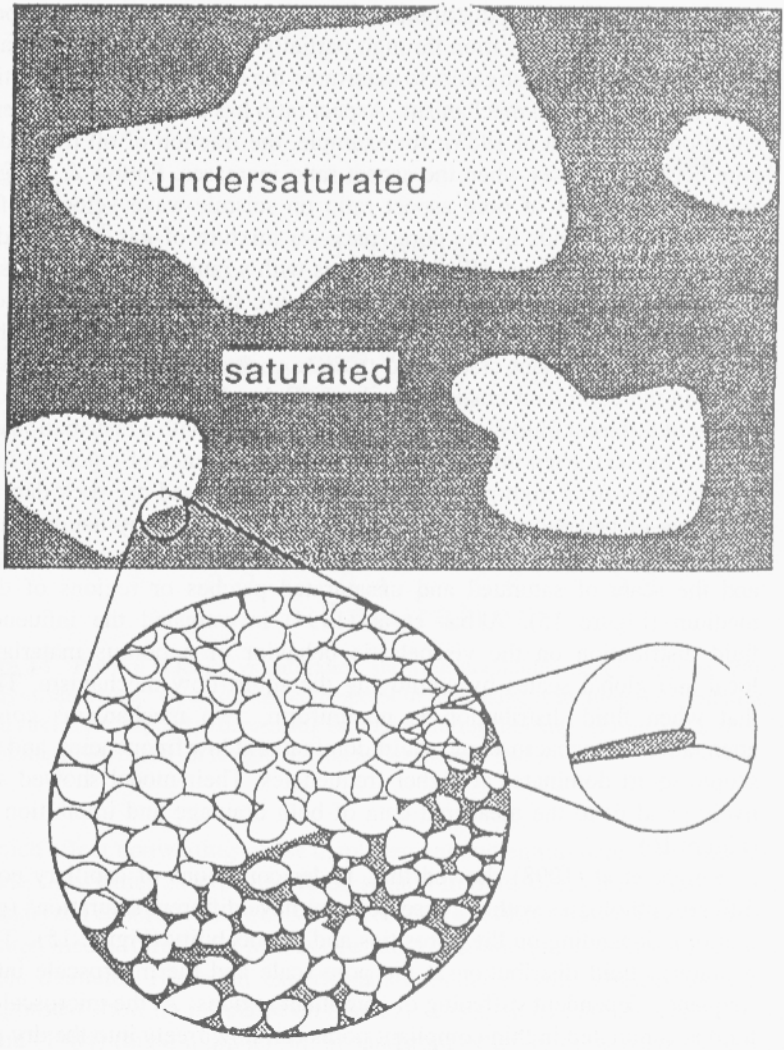

Figure 15 Concept of "patchy" saturation. The thinnest, compliant parts of the pore space can be wetted throughout the rock, but on much larger scales some patches of the rock are undersaturated while other patches are fully saturated. (From Mavko & Nolen-Hoeksema 1994.)

TOMOGRAPHIC IMAGING OF RESIDUAL HYDROCARBON IN WATER-SATURATED SEDIMENTS

Introduction

The detection of migration of an immiscible phase through a porous medium is an important task in oil and gas production, as well as in monitoring subsurface

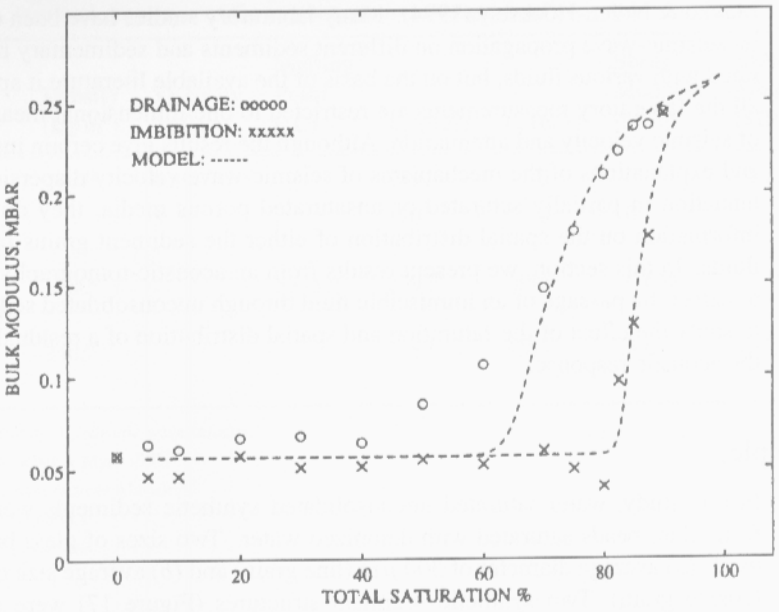

Figure 16 Bulk modulus calculated from measured V_p and V_s vs total water saturation for drainage and imbibition in tight gas sandstone using local and global squirt-flow theory (dashed line). The experimental data points are from Knight & Nolen-Hoeksema 1990. (From Akbar et al 1994.)

contamination. Laboratory studies have shown that as an immiscible fluid phase migrates through a saturated porous medium, it leaves residue in the pore space or at grain contacts. In shallow sediment aquifers, the sediment structure may be disturbed by the motion of the fluid during flow (e.g. grain compaction or separation). On the macroscale, the flow of immiscible fluids in a porous medium results in uneven saturation that is caused by the heterogeneity of the sediment structure (i.e. the spatial and size distribution of grain size and shape, porosity, and permeability) and by the difference in the flow rates, viscosities, and densities of the fluid phases. All of these effects result in an alteration of the elastic properties of the porous medium. Changes in the elastic properties of a porous medium will affect the properties of acoustic waves. As shown in the previous sections of this paper, the acoustic properties of a porous medium depend on the elastic moduli of the porous medium (Dvorkin et al 1994b, Ecker et al 1998), the bulk modulus of the pore fluid (Knight & Nolten-Hoeksema 1990), and the interaction between the solid and fluid (Biot 1956a,b, 1962; O'Connell & Budiansky 1977; Clark et al 1980). Thus, in principle, seismic data should indicate the passage of an immiscible fluid through a porous medium. However, the location of the immiscible fluid phase within the pore (at grain contact or in the center of the pore) and the distribution of the immiscible fluid phase in the sample (homogeneous saturation or patchy saturation) also impact the seismic-wave response (Akbar et al 1994,

Mavko & Nolen-Hoeksema1994). Many laboratory studies have been conducted on seismic-wave propagation on different sediments and sedimentary rocks saturated with various fluids, but on the basis of the available literature it appears that all the laboratory measurements are restricted to one-dimensional measurements of seismic velocity and attenuation. Although the results give certain insights into and explanations of the mechanisms of seismic-wave velocity dispersion and attenuation in partially saturated or unsaturated porous media, they do not yield information on the spatial distribution of either the sediment grains or the pore fluids. In this section, we present results from an acoustic-tomography approach to detect the passage of an immiscible fluid through unconsolidated sediment and to study the effect of the saturation and spatial distribution of a residual phase on the acoustic response.

Samples

In this study, water-saturated unconsolidated synthetic sediments were created from glass beads saturated with deionized water. Two sizes of glass beads were used: (*a*) average diameter of 300 μm (fine grain) and (*b*) average size of 640 μm (coarse grain). Two synthetic sediment structures (Figure 17) were packed in plastic cylindrical containers measuring 220 mm in diameter and 200 mm in height. The samples included (*a*) a homogeneous sample composed of coarse grain beads and (*b*) a sample composed of vertical coarse-grain columns embedded in a fine-grain matrix. The immiscible fluid used in these experiments was molten paraffin. The physical properties of soda-lime glass beads, paraffin, and water are listed in Table 1. A block with a mixture of solidified paraffin and glass beads was placed at the bottom of the sediment.

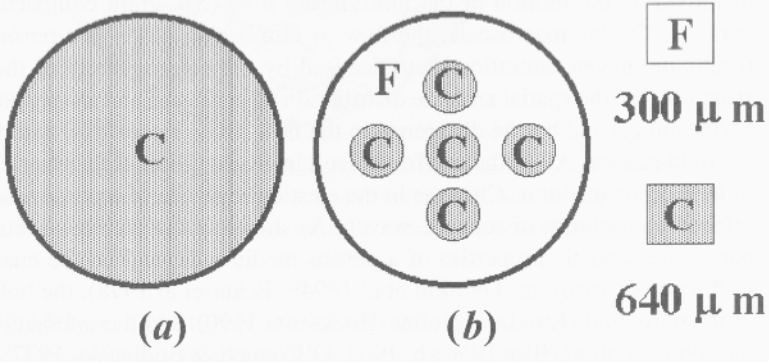

Figure 17 Two idealized sediment structures were created from soda-lime glass beads; two sizes of glass bead were used: 300 μm (fine grain) and 640 μm (coarse grain). Homogeneous coarse grain (*a*) and vertical coarse-grain (*b*) columns were embedded in a fine-grain matrix.

TABLE 1 Physical properties of the synthetic sediments and fluid[a]

Substance	Density (kg/m^3)	Viscosity (mPa s)	Melting Point (°C)	V_p (m/s)	V_s (m/s)	Shear Modulus (MPa)	Bulk Modulus (MPa)
Water	997[b]	0.890[b]		1497[b]	0	0	2.250[b]
Paraffin (100°C)		3.7[c]		1201[d]	0	0	
Paraffin (solidified)	900[c]		53–57[c]	2097[d]	842[d]	0.638[d]	3.107[d]
Soda-lime glass	2405[e]			6789[e]	3263[e]	25.6[e]	76.71[e]

[a]V_p, p-wave velocity; V_s, seismic-wave velocity.
[b]Data are from Geller & Myer 1995.
[c]Data are from manufacturer Aldrich.
[d]Measured by the authors.
[e]Data are from Press 1966.

Samples were heated for 3 days at a constant temperature of 85°C to allow the paraffin to melt and to flow through the sample. A nominal load was place on the top of each sediment samples to prevent the heaving of the sediment during the density-driven flow. After the sample cooled down to room temperature and the residual paraffin solidified, acoustic tomography was used to image a cross-section of the sample.

Experimental Setup and Procedure

Acoustic measurements were made with an acoustic tomographic imaging system. The system (Figure 18) is composed of a high-voltage pulse generator (IRCO model M1K-20), an oscilloscope (Lecroy Co. model 94136), two computer-controlled rotary stages (Newport Co. model URM100PP and Motion Master 2000), two to four water-coupled broadband plane-wave piezoelectric transducers (Panametrics Co.) with a central frequency of 1 MHz, and a barrel to hold the sample and water (the fluid coupling the transducers and the sample). The pulse generator generates a square pulse with an output of ~100–400 V with a width of 400 ns and a repetition rate of 100 Hz. The oscilloscope can record up to four channels concurrently. Immersion transducers were used to ensure uniform coupling of the transducer and sample at different sampling locations. One transducer was used as a source to send out the acoustic signals; the other transducers were used to receive the acoustic signals after the signal had passed through the sample. The transmitted signal was recorded every 5° for 46 receiver positions, resulting in a scan fan with 230° coverage per source position. Sixty-eight source positions were used for a total of 3128 waveforms.

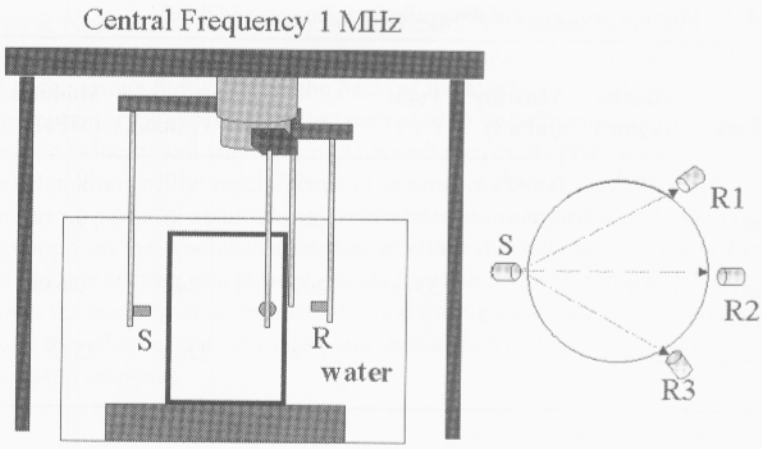

Figure 18 Experimental apparatus and data collection. Water-coupled piezoelectric transducers (1 MHz) were used to send and receive acoustic signals. Two computer-controlled rotary stages were used to move the source and the three receivers, independently, in 5° increments. Time-of-flight tomography was used to reconstruct several cross-sections of the sample.

To investigate the effect of paraffin migration on the acoustic response of a sample, experiments to measure the acoustic characteristics of the sediments pre- and postheating were performed at 25°C. A two-dimensional time-of-flight technique (Brzostowski & McMechan 1992) was used to reconstruct a cross-section of both sediment samples. The reconstruction quantity was the differential apparent attenuation; in other words, for each postheating experiment; the first peak-to-peak amplitude of the signal was normalized by the preheating peak-to-postheating peak amplitude at the same source-receiver location. The inverse of this ratio was used to solve for differential attenuation.

After the acoustic measurement was performed, the sediment with residual paraffin was excavated and analyzed by subvolumes to determine the concentration of residual paraffin. At each depth, the sample was sectioned into ~100 voxels by using a rectangular grid with a depth of 8 mm. A gravimetric technique was used to determine the residual-paraffin concentration of sample. Each subvolume of sediment was bathed in hexane to dissolve the residual paraffin. The volume fraction of the residual wax is obtained from the equation $f_p = W_p/(W_s\rho_s\phi)$, where f_p is the volume fraction of residual paraffin, W_p is the weight of the residual paraffin, W_s is the weight of the dried sediments, ρ_s is the density of the sediments, and ϕ_s is the porosity of the sediments. The residual-paraffin concentration maps are compared with the acoustic tomograms at each sample depth to examine the effect of saturation and the effect of the spatial distribution of the residual paraffin on acoustic-wave propagation. The microscopic spatial distribution of paraffin within the pores and at grain contacts was examined by scanning electronic microscopy (SEM).

Results and Analysis

Paraffin Flow in Homogeneous Sediments Acoustic tomography was performed at several depths of the homogeneous coarse-grain sediment sample (sample *a*) before and after paraffin flow through. The acoustic signals changed significantly after paraffin migrated though the sediment. Figure 19*a* (see color insert) shows the relative effective attenuation tomogram of a cross-section of sample *a*. The term "relative" means that the tomogram was reconstructed on the basis of the ratio of the pre- and post-paraffin-flow signal amplitudes. At the same depth as the acoustic measurements, a residual-paraffin concentration map was obtained by excavating the sample [Figure 19*b* (see color insert)]. The relative attenuation data were compared with the distribution of residual paraffin. The paraffin concentration values are volume percentages of paraffin residue in the pore space. For this sample, the overall residual-paraffin concentration is low (<1%). Most of the paraffin was observed to migrate to the top of the sample; only a small amount of residual paraffin was left in the pores. Figure 19*b* (see color insert) shows that, within the sampled cross-section, the outer regions of the sample have a relatively higher residual-paraffin concentration (~0.5%) than the central regions (<0.01%). In the central region, the amount of paraffin residue was relatively low but corresponded to a region with a high relative acoustic attenuation; in other words, the amplitude of the signal decreased relative to the pre-paraffin-flow state. The relative acoustic attenuation in the outer regions is lower than the attenuation observed in the center of the sample. SEM was performed on the paraffin-contaminated glass beads to visually inspect the spatial distribution of paraffin within the pore space. The samples were taken from a depth not analyzed for paraffin concentration. Two residual-paraffin distribution patterns, corresponding to different acoustic signature of the sediments, were observed: thin paraffin bridges and small patches of paraffin.

Thin bridges of paraffin between sediment grains (Figure 20*a*) occurred mainly in the outer regions of the sample, where the paraffin residual content was relatively high (~0.5%). The paraffin partially coated the surface of the grains and formed a bridge between the two beads. Behind the bridge, no paraffin was observed. It was hypothesized that the paraffin bridge behaved like a soft cement and stiffened the contact of the grain, which can result in an increase in the bulk modulus of the sediment (Dvorkin et al 1991, 1994b) and increase seismic-wave amplitude.

Unevenly distributed small patches of paraffin on the surface of the grain (Figure 20*b*) were found in the central regions of the sample, where the residual paraffin concentration is low (<0.01%). The paraffin was observed to be unevenly distributed on the surface of the grain, forming tiny spots as surface contamination (Figure 20*b*). It is known that changing the surface properties of grains affects the physicochemical interaction between the grain surface and pore water (Moerig 1996), which results in changes in the grain surface energy. This may be a mechanism that contributes to the high-level seismic attenuation observed in the regions with small-patch paraffin distribution.

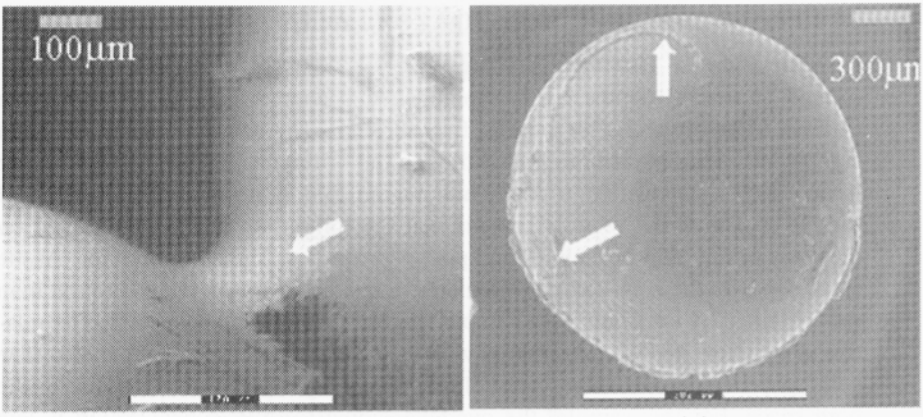

Figure 20 SEM micrographs of the distribution of the residual wax on the surface of the glass beads. (*a*) In the regions with low attenuation and high wax concentration, the residual wax formed thin bridges between two beads. The bridge behaved like soft cement, which can strengthen the contact stiffness and increase the bulk modulus. (*b*) In the regions with high attenuation and low wax concentration, the residual wax was unevenly distributed on the bead surface, which indicates variable wettability.

Sediment Structure Control of Paraffin Flow In sample *b*, two sizes of sediment were used in packing the sample. The cross-sections of the samples were imaged before and after the flow of paraffin with the goals of (*a*) delineating the sediment structure, (*b*) determining the paraffin flow path, and (*c*) detecting the residual-paraffin saturation.

In the acoustic tomogram obtained before the flow of paraffin, only the boundaries between the regions with different grain sizes can be (barely) discerned as the yellow regions (Figure 21*b*, see color insert) of the relative attenuation tomogram for sample *b*. After the paraffin flow was applied, regions with different grain sizes had different acoustic responses (Figure 21*c*). The acoustic energy is highly attenuated (red regions in Figure 21*c*) and the acoustic velocity is increased in the coarse-grain region compared with the pre-paraffin-flow tomogram. In the fine-grain regions of the sample, there are no major changes in acoustic responses pre- and post-paraffin flow. Comparing the acoustic tomogram with the residual-paraffin concentration map (Figure 21*d*, see color insert), it is observed that regions with high-level effective seismic attenuation correspond to regions with high paraffin residue concentrations; in other words, a 0.8-cm^{-1} increase in effective attenuation corresponded to a 15% volume of residual paraffin. Regions with low-level seismic attenuation were observed to correspond to regions with low residual-paraffin concentrations. These observations suggest that molten paraffin flowed predominantly in the highly permeable coarse-grain portions of the sediments.

The spatial distribution of paraffin within the pores was examined by optical microscopy and SEM. "Fine fingers" of paraffin (i.e. the residual paraffin filled only the center of pore space and left the grain contact region unfilled) were observed in coarse-grain regions of the sample (Figure 22). In the fine-grain size regions, no paraffin, or only a tiny amount of paraffin, was found on the surface of the grain.

Paraffin Saturation versus Seismic Response To study and verify the acoustic behavior observed in the acoustic tomograms, control experiments were performed on smaller samples to study the effect of residual-paraffin saturation on wave propagation. Acoustic mapping was performed on samples with a diameter of 31 mm (Figure 23*a*). In acoustic mapping, the source and receiver are diametrically opposed and are moved concurrently to sample the change in acoustic-wave velocity and amplitude as a function of position. The paraffin was assumed to be distributed uniformly at a given depth and within a particular cross-section. The acoustic velocity of sediments without paraffin is ~1730 m/s. Figure 23*b* shows the differential seismic velocity as a function of the residual-paraffin concentration. The acoustic-wave velocity increased monotonically with increasing residual paraffin in the pore space.

Dvorkin's contact cementation model (Dvorkin et al 1991, 1994b), a modified Voigt-Reuss-Hill model (Dvorkin & Nur 1996), and Kuster's inclusion model

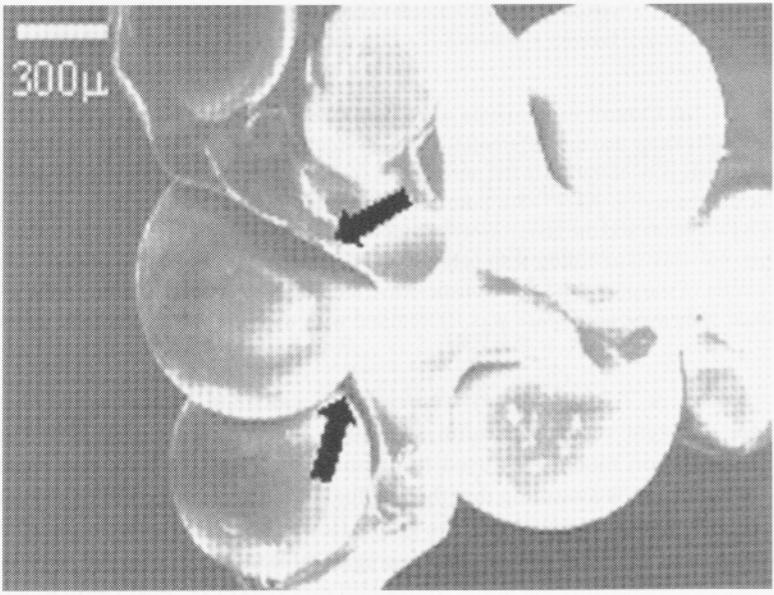

Figure 22 SEM micrographs of the residual paraffin in the pore. The paraffin formed "fine fingers"; that is, it filled only the center of pore space, leaving the grain contact region unfilled.

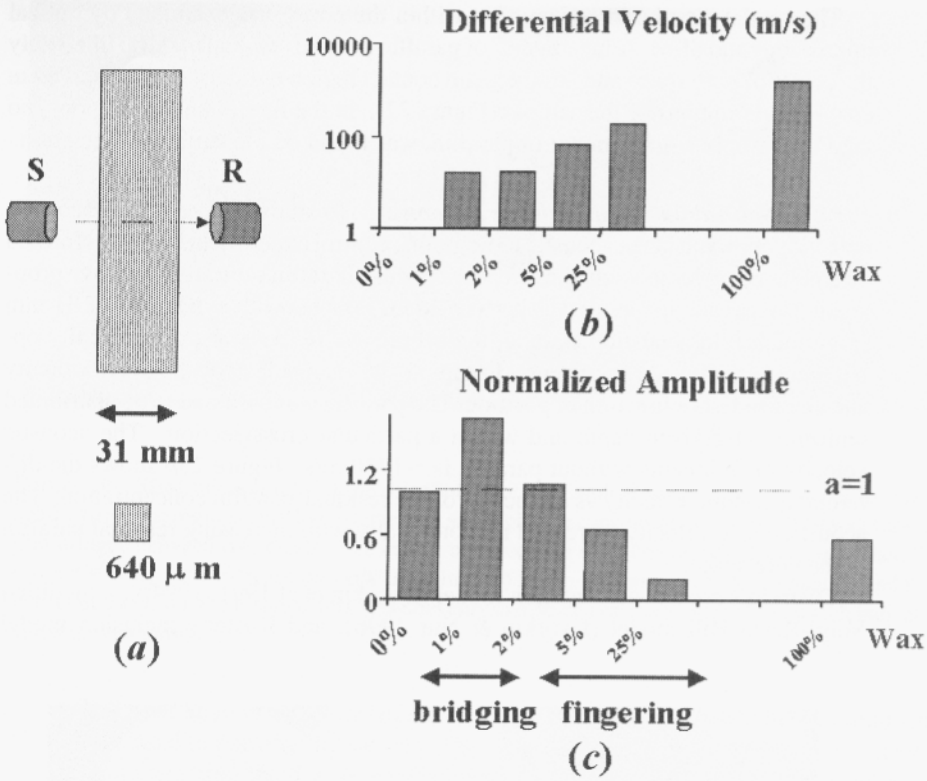

Figure 23 (*a*) Control experiments were performed on samples with a diameter of 31 mm. (*b*) The results show that the differential seismic velocity monotonically increased with an increase in residual wax concentration in the pore space. (*c*) However, the wave amplitude exhibited a more complicated behavior. At ~1–3% pore filling, the wax residue formed bridges (see Figure 20*a*) between two beads and the acoustic-wave amplitude increased relative to the pre-wax-flow amplitude. At ~5–40% pore filling with paraffin, the residual wax formed thin fingers (see Figure 22) in the center of the pores and the acoustic-wave amplitude decreased relative to the pre-wax-flow amplitude. When the pore space was 100% filled with wax, the wave amplitude increased.

(Kuster & Toksoz 1974a) were used to calculate the acoustic-wave response for different residual-paraffin saturation levels (Figure 24). Dvorkin's contact cementation model was used to estimate the effective bulk and shear modulus of the dry rock assuming that the residual paraffin is concentrated at grain contacts (upper bound) or envelopes the grains (lower bound). Residual paraffin is treated as part of the solid phase. The averaged bulk modulus of solid phase, K_s, is also calculated by using the Voigt-Reuss-Hill average (Ecker et al 1998) for comparison:

$$K_s = \frac{1}{2}\left\{ fK_g + (1-f)K_p + \left[\frac{f}{K_g} + \left(\frac{1-f}{K_p}\right)\right]^{-1}\right\},$$

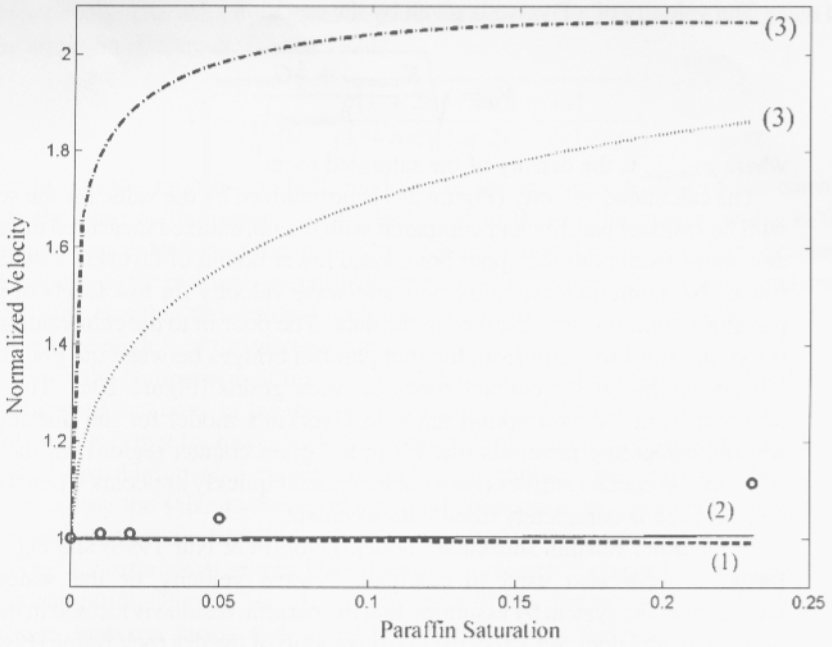

Figure 24 Normalized velocity as a function of residual saturation. Circles represent the experimental data; lines are theoretical calculations from (1) Kuster's inclusion model, (2) a modified Hashin-Shtrikman model, and (3) Dvorkin's contact cementation model (upper and lower bounds).

where K_g and K_p are the bulk moduli of the glass beads and paraffin, respectively, and f is the volume fraction of the glass beads in the solid phase.

The effective bulk and shear moduli of the water-saturated rock were also calculated for comparison, using Gassmann's (1951) formulas (from Ecker et al 1998):

$$K_{\text{saturated}} = K_s \frac{\phi K_{\text{dry}} - \frac{(1+\phi)K_f K_{\text{dry}}}{K_s} + K_f}{(1-\phi)K_f + \phi K_s - \frac{K_f K_{\text{dry}}}{K_s}},$$

and

$$G_{\text{saturate}} = G_{\text{dry}},$$

where K_{saturate} and G_{saturate} are the bulk and shear moduli of the saturated rock, respectively; K_{dry} and G_{dry} are the bulk and shear moduli of the dry rock, respectively; K_f and G_f are the bulk and shear moduli of the fluid phase, respectively; K_s and G_s are the bulk and shear moduli of the solid phase, respectively; and ϕ is the porosity of the rock.

The velocity of a P wave is given by the equation

$$V_{\mathrm{p}} = \sqrt{\frac{K_{\mathrm{saturate}} + \frac{4}{3}G_{\mathrm{saturate}}}{\rho_{\mathrm{saturate}}}},$$

where ρ_{saturate} is the density of the saturated rock.

The calculated velocity (Figure 24) is normalized by the value for the sediment with no residual paraffin and compared with the normalized measured data. Large deviations from both the upper bound and lower bound of Dvorkin's model were found. No rapid increase in the acoustic-wave velocity for low levels of residual paraffin saturation was observed in the data. The poor fit to the cementation model is hypothesized to result from the thin paraffin bridges between the grains, which left no paraffin at the contact zones between grains (Figure 20*a*). This is very different from the assumption made in Dvorkin's model for the distribution of wetting cementing materials that fill in the grain contact regions. In the case of paraffin, the contact stiffness may not increase as quickly as occurs when the whole contact zone is completely filled with a cement.

A modified Hashin-Shtrikman model (Dvorkin & Nur 1996) and Gassmann's formulas were also used to calculate P-wave velocity of the water-beads-paraffin residue system by assuming that the paraffin residue is located in the center of the pore and does not affect the elastic moduli of the dry rock frame (Figure 24). The contacts of the grain are calculated from the Hertz-Mindlin contact theory. The paraffin is treated as part of the fluid phase, and the fluid-phase bulk modulus (K_{fluid}) is calculated by using the Reuss average (from Ecker et al 1998),

$$K_{\mathrm{fluid}} = \left(\frac{S}{K_{\mathrm{p}}} + \frac{1-S}{K_{\mathrm{w}}}\right)^{-1},$$

where K_{w} is the bulk modulus of water and S is the residual saturation. The calculated result shows that the residual saturation causes only a small increase in velocity owing to the increase of the average bulk modulus of the fluid phase. This model underestimated the velocity increase rate, which might suggest that part of the residual paraffin does affect the grain contact stiffness, but not to the extent of a soft cement.

In Kuster's inclusion model, the fluid phase is the matrix and the solid phase is the inclusion. The residual paraffin is treated as the fluid phase, and the average bulk moduli and density of the matrix are calculated from the equations

$$K_{\mathrm{matrix}} = SK_{\mathrm{p}} + (1-S)K_{\mathrm{w}}$$

and

$$\rho_{\mathrm{matrix}} = S\rho_{\mathrm{p}} + (1-S)\rho_{\mathrm{w}},$$

where K_{matrix}, K_{p}, and K_{w} are the bulk moduli of the fluid, paraffin, and water, respectively, and ρ_{matrix}, ρ_{p}, and ρ_{w} are the density of the fluid, paraffin, and water,

respectively. The velocity normalized to a zero inclusion concentration is given by the equation (Kuster & Toksoz 1974)

$$V_p = \sqrt{\frac{b[1 + 2r - 2c(1 - r)]}{[b + (1 - b)c][1 + 2r - c(1 - r)]}},$$

where b is the ratio of the bulk modulus of the inclusion to that of the matrix, r is the ratio of the density of the inclusion to that of the matrix, and c is the volume concentration of the inclusions. Kuster's model predicts a slight decrease in velocity as the residual saturation increases, which is opposite the measured data. This suggests that the residual paraffin affects the rock frame, thereby affecting the elastic moduli of the water-saturated rock.

From the comparison of the measured data with all three theoretical models, it is observed that none of the theories reasonably predicts the experimental results. This suggests that for heavy hydrocarbon-bridging cements, the amounts and local spatial distribution of a cement around grain contacts are important factors in determining the seismic-wave velocity and attenuation in a porous medium with residual phase saturation.

The acoustic-wave amplitude exhibits complicated behavior as a function of wax saturation (Figure 23). At ~1–3% pore filling, the residual paraffin formed bridges between beads and strengthened the contact stiffness of the sediment grains. The acoustic-wave amplitude for these low concentrations increased compared to that of sediments without paraffin. For a paraffin saturation of ~5–25%, the residual paraffin formed thin fingers in the center of the pores. The acoustic-wave amplitude decreased compared to that of the sediment sample without paraffin. The fingers became fatter with increasing paraffin concentration. Figure 25

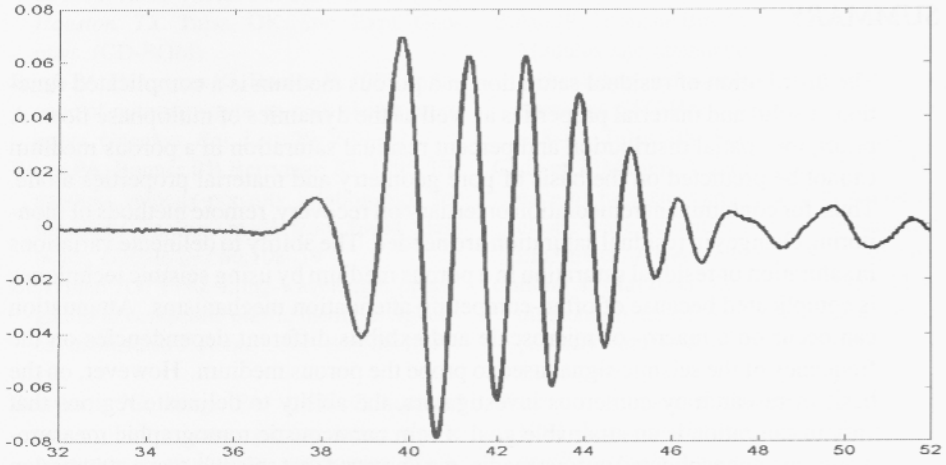

Figure 25 A transmitted wave signal from a control sample with ~3% residual saturation. The oscillations after the first cycle are evidence of scattering.

shows a transmitted wave signal obtained when the residual saturation was ~3%. Generally, the oscillation in amplitude of the later arrival is evidence of scattering. Seismic energy can be scattered from inclusions as well as at interfaces of a residual paraffin-water-grain system. The wavelength in the experiment is ~5 mm. If the size of the inclusion is larger than 500 μm in diameter, the propagating wave will be strongly scattered (Geller & Myer 1995). However, if the presence of residual paraffin in the pore increased the apparent number of contact planes, according to the displacement-discontinuity theory (Pyrak-Nolte et al 1990, Nihei 1992) more seismic energy will be scattered. As a result, the size of the paraffin finger may cause more wave scattering and result in a reduction of acoustic-wave amplitude. When the pore space is nearly 100% filled with paraffin, the sediments were cemented together and behaved like a solid, which resulted in an increase in acoustic-wave amplitude.

The velocity and amplitude results show that two competing factors act on the propagating wave at the same time: an increase in grain contact stiffness caused by residual paraffin acting as a weak cement and a decrease in the transmitted energy caused by scattering. The velocity data suggest that the heavy hydrocarbon cements may produce attenuation and velocity behaviors different from those of common wetting-cementing materials, such as ice or epoxy, used in other experimental work. Further investigation is needed in terms of modeling the contact stiffness of grains with a cement that forms bridges. The amplitude data indicate that scattering is an important attenuation mechanism at ultrasonic frequencies. They also demonstrate that the local distribution of the residual paraffin in the pore and at grain contacts appears to have a greater effect on seismic-wave propagation than global saturation.

SUMMARY

The distribution of residual saturation in a porous medium is a complicated function of solid and material properties as well as the dynamics of multiphase flow. A priori, the spatial distribution and percent residual saturation in a porous medium cannot be predicted on the basis of pore geometry and material properties alone. Thus, for contaminant remediation or tertiary oil recovery, remote methods of monitoring changes in residual saturation are needed. The ability to delineate variations in saturation or residual saturation in a porous medium by using seismic techniques is complicated because of often-competing attenuation mechanisms. Attenuation can occur on a macro- or microscale and exhibits different dependencies on the frequency of the seismic signal used to probe the porous medium. However, on the basis of research by numerous investigators, the ability to delineate regions that vary in saturation is an attainable goal. From our acoustic tomographic measurements on unconsolidated porous media, we observed that seismic-wave attenuation is sensitive to alteration of the grain contact stiffness even for only a few percent residual phase saturation and to spatial features (bridging between grains) that are

~1/100 of a wavelength. Thus, the effect of microscale phenomena on macroscale measurements of seismic-wave attenuation and velocity cannot be ignored.

ACKNOWLEDGMENTS

We acknowledge the support of this research by the Geosciences Research Program, Office of Basic Energy Sciences, and the US Department of Energy, and equipment support from the National Science Foundation (9521686-CMS). LJP-N acknowledges support from National Science Foundation Young Investigator awards (EAR-9896057 and EAR-9458373).

LITERATURE CITED

Akbar N, Dvorkin J, Nur A. 1993. Relating P-wave attenuation to permeability. *Geophysics* 58:20–29

Akbar N, Mavko G, Nur A, Dvorkin J. 1994. Seismic signatures of reservoir transport properties and pore fluid distribution. *Geophysics* 59:1222–36

Bacri JC, Salin D. 1986. Sound velocity of a sandstone saturated with oil and brine at different concentrations. *Geophys. Res. Lett.* 13(4):326–28

Batzle M, Han D, Castagna J. 1999. Fluids and frequency dependent seismic velocity of rock. *Abstr. Annu. Int. SEG Meet., 69th, Houston, TX.* Tulsa, OK: Soc. Expl. Geophys. (CD-ROM)

Berge PA, Berryman JG, Bonner B. 1993. Influence of microstructure on rock elastic properties. *Geophys. Res. Lett.* 20:2619–22

Berge PA, Bonner BP, Berryman JG. 1995. Ultrasonic velocity-porosity relationships for sandstone analogs made from fused glass beads. *Geophysics* 60:108–19

Berryman JG. 1980. Long-wavelength propagation in composite elastic media. I. Spherical inclusions. *J. Acoust. Soc. Am.* 68:1809–19

Berryman JG, Berge PA. 1996. Critique of two explicit schemes for estimating elastic properties of multiphase composites. *Mech. Mater.* 22:149–64

Biot MA. 1956a. Theory of propagation of elastic waves in a fluid saturated porous solid. I. Lower-frequency range. *J. Acoust. Soc. Am.* 28:168–78

Biot MA. 1956b. Theory of propagation of elastic waves in a fluid saturated porous solid. II. Higher-frequency range. *J. Acoust. Soc. Am.* 28:179–91

Biot MA. 1962. Generalized theory of acoustic propagation in porous dissipative media. *J. Acoust. Soc. Am.* 34:1254–64

Brzostowski M, McMechan G. 1992. 3-D tomographic imaging of near surface seismic velocity and attenuation. *Geophysics* 57:396–403

Bulau JR, Tittmann BR, Abdel-Gawad A. 1984. Modulus and attenuation in sandstone with hydrocarbon and aqueous pore fluids. *Abstr. Annu. Int. SEG Meet., 54th*, Atlanta, GA, pp. 658–61. Tulsa, OK: Soc. Expl. Geophys.

Cadoret T, Marion D, Zinszner B. 1995. Influence of frequency and fluid distribution on elastic wave velocities in partially saturated limestones. *J. Geophys. Res.* 100:9789–803

Cadoret T, Mavko G, Zinszner B. 1998. Fluid distribution effect on sonic attenuation in partially saturated limestones. *Geophysics* 63:154–60

Chatzis I, Kuntamukkula MS, Morrow NR. 1984. *Blob-size distribution as a function of capillary number in sandstones, SPE 13213.* Presented at Annu. Techn. Conf. Exhib., 59th, Houston

Chatzis I, Morrow NR, Lim HT. 1983. Magnitude and detailed structure of residual oil saturation. *Soc. Petrol. Eng. J.* 23:311–26

Clark VA, Tittman BR, Spencer TW. 1980. Effect of volatiles on attenuation (Q^{-1}) and velocity in sedimentary rocks. *J. Geophys. Res.* 85:5190–98

Cleary MP, Chen IW, Lee AM. 1980. Self-consistent techniques for heterogeneous media. *J. Eng. Mech. ASCE* 106:861–87

Dawson HE, Roberts PV. 1997. Influence of viscous, gravitational, and capillary forces on DNAPL saturation. *Ground Water* 35:261–69

Devaney AJ. 1980. Multiple scattering theory for discrete, elastic, random media. *J. Math. Phys.* 21:2603–11

Dvorkin J, Berryman J, Nur A. 1999. Elastic moduli of cemented sphere packs. *Mech. Mater.* 31:461–69

Dvorkin J, Mavko G, Nur A. 1991. The effect of cementation on the elastic properties of granular material. *Mech. Mater.* 12:207–17

Dvorkin J, Nolen-Hoeksema R, Nur A. 1994a. Squirt-flow mechanism: macroscopic description. *Geophysics* 59:428–38

Dvorkin J, Nur A. 1993. Dynamic poroelasticity: a unified model with the squirt and the Biot mechanisms. *Geophysics* 58:524–33

Dvorkin J, Nur A. 1996. Elasticity of high-porosity sandstones: theory for two North Sea data sets. *Geophysics* 61:1363–70

Dvorkin J, Nur A, Yin H. 1994b. Effective properties of cemented granular material. *Mech. Mater.* 18:351–66

Ecker C, Dvorkin J, Nur A. 1998. Sediments with gas hydrates: internal structure from seismic AVO. *Geophysics* 63:1659–69

Elektorowicz M, Konyukhov B. 1995. Dynamic mapping of contaminated sediments by the boundary wave modulation method. *Environ. Technol.* 16:595–601

Endres AL, Knight R. 1991. The effects of pore scale distribution of fluids on the physical properties of partially saturated tight sandstones. *J. Appl. Phys.* 69:1091–98

Galvez R. 1989. *Clay suspension as a buffering system for accumulation of lead as a soil pollutant*. Master's thesis. McGill Univ.

Gassmann F. 1951, Uber die elastizitat poroser Medien. *Vierteljahresschr. Naturforschenden Ges. Zür.* 96:1–23

Geller JT, Myer LR. 1995. Ultrasonic imaging of organic contaminants in unconsolidated porous media. *J. Contam. Hydrol.* 19:85–104

Gordon RB. 1974. Mechanical relaxation spectrum of crystalline rock containing water. *J. Geophys. Res.* 79:2129–31

Hamilton EL. 1972. Compressional-wave attenuation in marine sediments. *Geophysics* 37:620–46

Hashin Z. 1962. The elastic moduli of heterogeneous materials. *J. Appl. Mech. ASME* 29: 143–50, 765–66

Hill R. 1952. The elastic behavior of a crystalline aggregate. *Proc. Phys. Soc. Lond. Ser. A* 65:213–22

Hoag GE, Marley MC. 1985. Gasoline residual saturation. I. Unsaturated uniform aquifer materials. *J. Environ. Eng.* 112(3):587–605

Hudson JA. 1981. Wave speeds and attenuation of elastic waves in material containing cracks. *Geophys. J. Int.* 102:485–90

Hudson JA. 1990. Attenuation due to second-order scattering in material containing cracks. *Geophys. J. Int.* 102:485–90

Ivanov AG. 1939. Effect of electrization of earth layers by elastic waves passing through them. *Dokl. Akad. Nauk SSSR* 24:42–45

Jones TD. 1986. Pore fluids and frequency-dependent wave propagation in rocks. *Geophysics* 51:1939–53

Jones TD, Nur A. 1983. Velocity and attenuation in sandstone at elevated temperature and pressure. *Geophys. Res. Lett.* 10:140–43

Klimentos T, McCann C. 1990. Relationships among compressional wave attenuation, porosity, clay content and permeability in sandstones. *Geophysics* 55:998–1014

Knight R, Dvorkin J, Nur A. 1998. Acoustic signatures of partial saturation. *Geophysics* 63:132–38

Knight R, Nolen-Hoeksema R. 1990. A laboratory study of the dependence of elastic

wave velocities on pore scale fluid distribution. *Geophys. Res. Lett.* 17:1529–32

Kuster GT, Toksoz MN. 1974a. Velocity and attenuation of seismic waves in two-phase media. I. Theoretical formulations. *Geophysics* 39:583–606

Kuster GT, Toksoz MN. 1974b. Velocity and attenuation of seismic waves in two-phase media. II. Experimental results. *Geophysics* 39:607–18

Larson RG, Davis HT, Scriven LE. 1981. Displacement of residual non-wetting fluid from porous media. *Chem. Eng. Sci.* 36:75–85

Lenormand R, Zarcone C. 1988. Physics of blob displacement in a two-dimensional porous medium. *SPE Form. Eval.* March: 271–75

Li X, Pyrak-Nolte LJ. 1998. Acoustic monitoring of sediment-pore fluid interaction. *Geophys. Res. Lett.* 25(20):3899–902

Mal AK, Knopoff L. 1967. Elastic wave velocities in two-component systems. *J. Instr. Math. Appl.* 3:376–87

Marion DP. 1990. *Acoustical, mechanical and transport properties of sediments and granular materials*. PhD. thesis. Stanford Univ., Palo Alto, CA

Mavko G, Jizba D. 1991. Estimating grain-scale fluid effects on velocity dispersion in rocks. *Geophysics* 56:1940–49

Mavko G, Nolen-Hoeksema R. 1994. Estimating seismic velocities at ultrasonic frequencies in partially saturated rocks. *Geophysics* 59:252–58

Mavko G, Nur A. 1979. Wave attenuation in partially saturated rocks. *Geophysics* 44:161–78

Mayer AS, Miller CT. 1992. The influence of porous medium characteristics and measurement scale on pore-scale distributions of residual non-aqueous-phase liquids. *J. Contam. Hydrol.* 11:189–213

McCann C, McCann DM. 1985. A theory of compressional wave attenuation in noncohesive sediments. *Geophysics* 50:1311–71

Miksis M. 1988. Effects of contact line movement on the dissipation of waves in partially saturated rocks. *J. Geophys. Res.* 93:6624–34

Moerig R. 1996. Seismic attenuation in artificial glass cracks: physical and physicochemical effects of fluids. *Geophys. Res. Lett.* 23(16):2053–56

Morrow NR, Chatzis I, Taber JJ. 1988. Entrapment and mobilization of residual oil in bead packs. *SPE Reserv. Eng.* Aug:927–34

Morrow NR, Songkran B. 1981. Effect of viscous and buoyancy forces on nonwetting phase trapping in porous media. In *Surface Phenomena in Enhanced Oil Recovery*, ed. DO Shah, pp. 1–246. New York: Plenum.

Murphy WF III, Winkler KW, Kleinberg RL. 1984. Frame modulus reduction in sedimentary rocks: the effect of adsorption on grain contacts. *Geophys. Res. Lett.* 1(9):805–8

Murphy WF III, Winkler KW, Kleinberg RL. 1986. Acoustic relaxation in sedimentary rocks: dependence on grain contact and fluid saturation. *Geophysics* 51:757–66

Ng KM, Davis HT, Scriven LE. 1978. Visualization of blob mechanics in flow through porous media. *Chem. Eng. Sci.* 33:1009–17

Nihei KT. 1992. *Micromechanics of seismic wave propagation in granular rocks*. PhD thesis. Univ. Calif., Berkeley. 167 pp.

Nur A, Simmons G. 1969. The effect of viscosity of a fluid phase on velocity in low porosity rocks. *Earth Planet. Sci. Lett.* 7:99–108

O'Connell RJ, Budiansky B. 1977. Viscoelastic properties of fluid-saturated cracked solids. *J. Geophys. Res.* 82:5719–36

Paffenholz J, Burkhardt H. 1989. Absorption and modulus measurements in the seismic frequency and strain range on partially saturated sedimentary rocks. *J. Geophys. Res.* 94:9493–507

Palmer ID, Traviolia ML. 1980. Attenuation by squirt flow in undersaturated gas sands. *Geophysics* 45:1780–92

Pennell KD, Pope GA, Abriola LM. 1996. Influence of viscous and buoyancy forces on the mobilization of residual tetrachloroethylene during saturation flushing. *Environ. Sci. Technol.* 30:1328–35

Press F. 1966. Seismic velocities In *Handbook*

of Physical Constants, ed. Clark SP Jr, pp. 195–218. New York: Geol. Soc. Am.

Pride SR, Morgan FD. 1991. Electrokinetic dissipation induced by seismic waves. *Geophysics* 56:914–25

Pyrak-Nolte LJ, Myer LR, Cook NGW. 1990. Transmission of seismic waves across single natural fractures. *J. Geophys. Res.* 95:8617–38

Reuss A. 1929. Berechnung der fliessgrense von mischkristallen auf grund der plastizitatbedingung fur einkristalle. *Z. Angew. Math. Mech.* 9:48–58

Scheidegger AE. 1974. *The Physics of Flow Through Porous Media*. Toronto: Univ. Toronto Press. 353 pp. 3rd ed.

Schroth MH, Istok JD, Ahearn SJ, Selker JS. 1995. Geometry and position of light nonaqueous-phase liquid lenses in water-wetted porous media. *J. Contam. Hydrol.* 19:269–87

Seifert P, Geller J, Johnson LR. 1998. Effect of P-wave scattering on velocity and attenuation in unconsolidated sand saturated with immiscible liquids. *Geophysics* 63:161–70

Shapiro SA, Zien H. 1993. The O'Doherty-Anstey formula and localization of seismic waves. *Geophysics* 58:736–40

Shapiro SA, Zien H, Hubral P. 1994. A generalized O'Doherty-Anstey formula for waves in finely layered media. *Geophysics* 59:1750–62

Stoll RD. 1974. Acoustic waves in saturated sediments. In *Physics of Sound in Marine Sediments*, ed. LD Hampton, pp. 19–39. New York: Plenum

Stoll RD. 1977. Acoustic waves in ocean sediments. *Geophysics* 42:715–25

Stoll RD, Bryan GM. 1970. Wave attenuation in saturated sediments. *J. Acoust. Soc. Am.* 47:1440–47

Tittman BR, Clark VA, Richardson JM, Spencer TW. 1980. Possible mechanism for seismic attenuation in rocks containing small amounts of volatiles. *J. Geophys. Res.* 85:5199–208

Tutuncu AN, Sharma MM. 1992. The influence of fluids on grain contact stiffness and frame moduli in sedimentary rocks. *Geophysics* 57:1571–82

Varadan VK, Ma Y, Varadan VV. 1989. Scattering and attenuation of elastic waves in random media. *Pure Appl. Geophys.* 131:557–603

Voigt W. 1910. *Lehrbuch der Kirstallphysik*. Leipzig, Ger.: Teubner

Walsh JB. 1965. The effect of cracks on the compressibility of rock. *J. Geophys. Res.* 41:621–45

Walsh JB. 1969. A new analysis of attenuation in partially melted rock. *J. Geophys. Res.* 74:4333–37

Wilson JL, Conrad SH. 1984. Is physical displacement of residual hydrocarbons a realistic possibility in aquifer restoration? *NWWA/API Conf. Petrol. Hydrocarb. Org. Chem. Groundw.*, pp. 144–56. Worthington, OH: Natl. Well Water Assoc.

Winkler KW. 1983. Contact stiffness in granular porous materials: comparison between theory and experiment. *Geophys. Res. Lett.* 10(11):1073–76

Winkler KW. 1985. Dispersion analysis of velocity and attenuation in Berea sandstone. *J. Geophys. Res.* 90:6793–800

Wu TT. 1966. The effect of inclusion shape on the elastic moduli of a two-phase material. *Int. J. Solids Struct.* 2:1–8

Wyllie MRJ, Gardner GHF, Gregory AR. 1962. Studies of elastic wave attenuation in porous media. *Geophysics* 27:569–89

Yamamoto T, Turgut A. 1988. Acoustic wave propagation through porous media with arbitrary pore size distributions. *J. Acoust. Soc. Am.* 83(5):1744–51

Zhong L. 1999. *Surfactant-enhanced nonaqueous phase liquid contaminant removal from liquid saturated media*. Ph.D. dissertation. Mich. Technol. Univ., Houghton.

Zhong L, Mayer AS, Glass RJ. 2000. Visualization of surfactant enhanced NAPL mobilization and solubilization in a two-dimensional micromodel. *Water Resour. Res.* In press

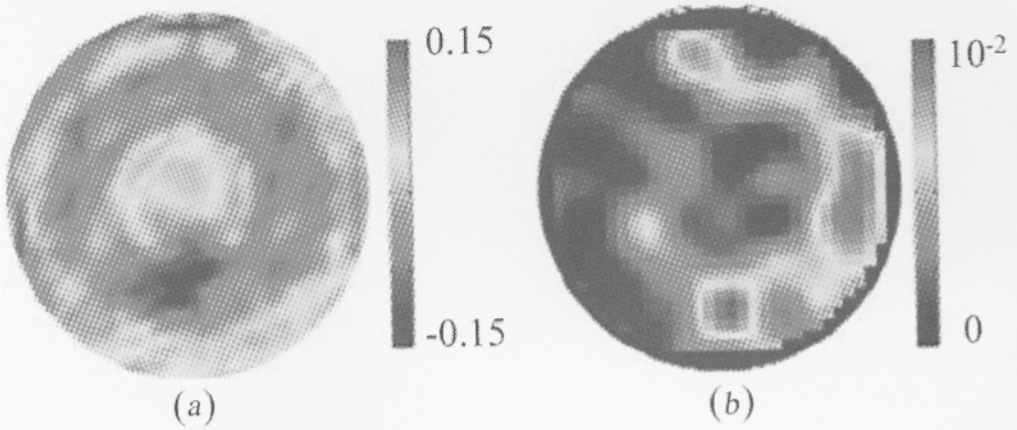

Figure 19 (*a*) The relative acoustic attenuation of a cross section of the homogenous coarse grain sample after wax flow. The color represents the magnitude of the attenuation (cm^{-1}) relative to pre-wax flow; (*b*) the residual wax concentration map obtained by excavation of the sample at the same depth as the acoustic measurements. The color represents the volume percentage of residual wax. Regions with low seismic attenuation were found to correspond to regions with high wax concentration.

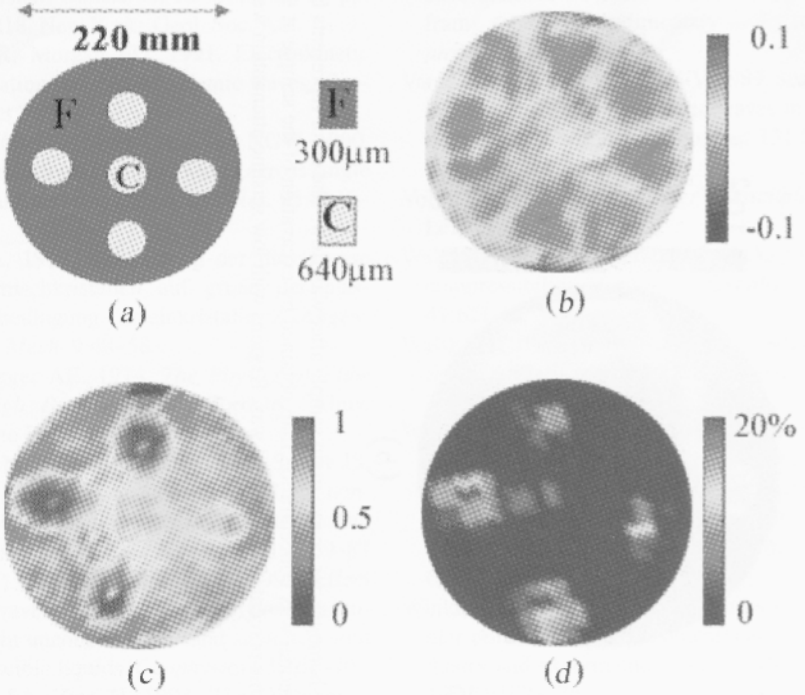

Figure 21 (*a*) Schematic diagram of the sample with vertical cylindrical sediment columns composed of coarse grains imbedded inside a sediment composed of fine grains; (*b*) the relative attenuation of a cross section of the fine grain column sample before paraffin flow. From the tomogram, only the boundaries between regions with different grain size can be barely discerned. (*c*) The relative attenuation of a cross section of the fine grain column sample after paraffin flow. Regions with high attenuation were found to correspond to the coarse grain portions of the sample. (*d*) The residual wax concentration map was obtained by excavation of the sample from the same depth at which the acoustic measurements were made. Regions with high seismic attenuation were found to correspond to regions with high wax concentration, which suggests that the wax predominantly flowed through the high permeability coarse regions.